



An Experimental Performance Evaluation and Management of a Dual Energy Storage System in a Solar Based Hybrid Microgrid

Akshit Samadhiya¹ · Kumari Namrata¹ · Nishant Kumar¹

Received: 9 March 2022 / Accepted: 5 June 2022 / Published online: 18 July 2022
© King Fahd University of Petroleum & Minerals 2022

Abstract

The paper proposes an energy management control scheme for a converter based hybrid AC–DC microgrid employing solar photovoltaic as the main power source. Dual energy storage system comprising of supercapacitodalr modules and battery bank act as auxiliary power source. Full bridge isolated DC–DC converter and dual active bridge bidirectional DC–DC converter are employed for photovoltaic system and energy storage system respectively while a neutral point clamped DC–AC converter is considered as the interface between distribution level power grid and DC-link. The overall control structure is categorized into photovoltaic side control including MPPT controller, grid side current control, energy management control and DC-link voltage regulation. Efficient power management is achieved through model predictive energy management control. High pass filtering based power sharing approach is employed for dual energy system to manage high frequency short duration transients for an effective DC voltage regulation. Grid side current controller is designed using two different approaches in stationary reference $\alpha\beta$ frame and synchronously rotating frame (dq) frame. Short term simulation based study is carried out in MATLAB/SIMULINK environment to assess the performance of the overall control structure under different operating and load conditions. Real time validation of the coordinated energy management control strategy is also presented using OPAL RT platform. The results suggest a better control in mitigating DC-link voltage ripple through proposed power sharing scheme. A deviation of 1.02% and 0.8 – 0.9% was observed in DC link voltage during start-up and under different loading conditions respectively. Additionally, the grid side controller designed using magnitude-frequency loop shaping in $\alpha\beta$ frame ensures better power quality at the point of common coupling as the total harmonic distortion in grid current is reduced to 1.65% for a synchronized grid participation.

Keywords Full bridge isolated DC–DC converter · Dual active bridge bidirectional DC–DC converter · Model predictive energy management control · Maximum power point tracking (MPPT) controller · Stationary reference ($\alpha\beta$) frame and synchronously rotating (dq) reference frame

1 Introduction

The global demand for electricity is expected to increase rapidly extrapolating its direct usage in agricultural sector, industries and residential applications [1]. It is expected

that the energy demand may rise about 2% per annum [2]. Rapid economic development, industrialization and population contributes towards annual growth in energy demand [3]. This demand is largely fulfilled by the conventional sources of energy dominated by coal and oil. Combustion of coal and oil results in carbon emission which may adversely effect the climatic pattern of the world [4]. Hence, a strategic shift is required to facilitate the development of low carbon renewable based technologies. This transition is focussed on implementation of cost effective and technically feasible solutions towards decarbonisation of the energy sector [5].

Since mid 20th century, the electric power industry was largely focussed on coal and oil fired power plants. During 21st century, attention has been paid towards integration of renewable based technologies into the existing power

✉ Kumari Namrata
namrata.ee@nitjsr.ac.in
Akshit Samadhiya
2018rsee007@nitjsr.ac.in
Nishant Kumar
2018rsee014@nitjsr.ac.in

¹ Department of Electrical Engineering, National Institute of Technology Jamshedpur, Jamshedpur 831014, Jharkhand, India



infrastructure [6]. The power system infrastructure needs transformation in all sections i.e generation, transmission and distribution to provide more flexibility, reliability and stability [2]. The concepts related to ‘Microgrid’, ‘High voltage DC transmission’, ‘Distributed generation’ and ‘Flexible AC transmission’ have revolutionized the power system industry.

Technically, microgrids and distributed generation systems have the potential to reshape the scalability and reliability of the existing power grid at a relatively lower cost of energy and environmental impact. Solar based DGs are quiet popular among other renewables due to the tremendous potential of solar energy as a resource, easy availability of raw materials to fabricate solar cells, low maintenance cost and decreasing trend in PV prices. The major issue to deal with wide scale adoption of solar based DGs is the intermittence in solar output generation due to daily or seasonal dependence on meteorological conditions. Thus, the energy transition is not only focussed on wide scale utilization of renewable energy but also on energy security and 100% energy access. Energy storage technologies ranging from short term to long term storage can eventually absorb the variable nature of renewable energy sources and thus play a crucial role during supply and demand mismatch [7].

Integration of solar based DGs into the main grid created a pathway to generate and supply electrical power near the load centres. While transferring electric power to the grid, certain strict integration requirements are being imposed by power system operators to maintain the stability and power quality of the grid. These grid integration requirements have a big impact on the design and analysis of photovoltaic based distributed generation systems. Organizations such as IEEE and IEC are among certain policy makers that frame technical standards, procedures and specifications to interconnect DGs into the main grid [8]. A microgrid should comply to these standards related to the safety of power converters, allowable limits of voltage and frequency variations, anti-islanding and power quality [9].

Microgrids can be categorized into AC type, DC type and hybrid AC–DC type based on nature of loads. Modern day power system has seen an increased penetration of DC loads. Applications including variable speed drives for industries, HVAC, tractions system, LED street lighting, power distribution in data centres, electrical vehicle (EV) charging requires DC supply for their operation [10]. Power electronics plays a vital role in conversion and control of power generated by renewable energy sources. Due to significant improvement in power semiconductor and microelectronics technologies, research works are focused on exploring the potential of power electronics in the field of power system [11,12].

The role of batteries and energy storage solutions will be crucial in defining the future of the energy system. With the focus on early adoption of EVs and renewable based technologies, the research in the field of batteries and its optimal

operation, control and management has gain popularity. Cost effective integration of batteries requires efficient energy management and proper control architecture to maximize battery lifetime. Hence, energy management is an important research aspects which focuses on economic operation of microgrid by effectively managing renewable energy sources and energy storage elements. Additionally, energy management controller also contribute towards effective regulation of DC link voltage profile .

Various microgrid architectures, power converter topologies, control techniques and energy management schemes have been adopted by researchers worldwide. Some of the researches related to the control, synchronization and energy management of renewable based ,microgrids has been reviewed. They have been listed in the Table 1.

Based on the literature review, following observations were drawn related to the power converter topologies , control , synchronization and energy management of Microgrids:-

- Power electronic converters are the core of photovoltaic based energy conversion Grid connected photovoltaic energy systems based on single stage and two stage conversion are practically employed. Buck and boost converters are widely employed for DC–DC conversion whereas voltage source converters are usually employed for DC–AC conversion.
- Photovoltaic generation side control includes maximum power point tracking (MPPT). MPPT technique controls the voltage and current of PV panel such that maximum power can be extracted
- Effective DC voltage regulation is required which may otherwise be responsible for propagation of power system disturbances between the microgrid and the main grid.
- Cascaded control loop structure is adopted for regulative the voltage and current injected into the grid. PI controllers are adopted in stationary reference frame while a PR controller is usually adopted in synchronously rotating reference frame.
- Phase locked loops (PLLs) are commonly employed for synthesizing the phase and frequency information of the power grid required for efficient synchronization.

Certain drawbacks have been identified in the literature survey:-

- The architecture based on conventional bidirectional controllers may not be suitable for high power applications considering wide scale deployment of renewable based technologies.
- High pass filtering based current sharing approach may not be enough to suppress the transients alone due to thermal limitation during battery’s charge and discharge cycle.



Table 1 Research works related to modeling, control and integration of renewable based microgrids

Authors	Methodology	Key findings/remarks
Xiao et. al. [13]	Authors described various topologies for grid connected photovoltaic inverter Power converter employed in different topologies are also discussed	Grid connected photovoltaic system can be divided into two categories:-central and distributed MPPT systems
Blaabjerg et. al [14]	Authors have addressed issues related to integration of distributed power generation system into the grid and role of power electronics converters for wind solar DGs.	Basic control strategies include MPPT, voltage/current control. Better power quality. Advance features include LVRT, DC voltage regulation, reactive/active power control under normal and abnormal conditions
Gee et. al [15]	Authors have proposed an off grid wind based energy system with battery and supercapacitor as storage options. Current sharing is based on filtering based approach	Results show that the supercapacitor supplies short term charging and discharging current which possibly enhances the lifetime of the battery
Kollimalla et. al [16]	Authors proposed an islanded DC microgrid with solar photovoltaics and windturbine as the main source while battery and supercapacitor as hybrid energy storage system in order to provide better voltage regulation	Result shows that the battery and supercapacitor not only helps maintaining the power balance in the system but also regulates the DC link voltage profile. Supercapacitor supplies short term power transients
Lin et. al [17]	Authors proposed a grid connected Wind based microgrid including hierarchical control of hybrid energy storage system	Result shows that the hybrid energy storage system is effective in smoothening the output of the wind farms. The effectiveness of the energy management controller based on fuzzy logic is also verified
Jami et. al [18]	Authors proposed a DC microgrid with PV as the main source while supercapacitor and battery as hybrid energy option.	Results show that the DC bus is regulated at 200 V under different loading condition. The virtual inertial control reduces the rate of change of DC voltage hence a better regulation is achieved
Takagi et. al [19]	The authors have developed a model to show the dynamic behaviour of a dual active bridge which are widely used in battery applications	Result verifies the transient response of converter during step variation in phase difference and effective DC voltage regulation is achieved using a PI Controller
Kong et. al [20]	The authors proposed a grid connected power system with PV as main power source, fuel cell as auxiliary source while supercapacitor and alkaline electrolyzers are employed as energy storage elements.	Result shows that the intermittence in solar output can be controlled by adopting co-ordinated power management strategy. Conventional boost and bidirectional converters are used for PV and storage elements respectively.
Senapati et al. [21]	The authors proposed an efficient energy management technique for a DC based microgrid including energy storage	Result shows the effective of the proposed scheme in regulating the DC link voltage under 1%. Takagi-Sugeno fuzzy control is used to improve the transient behaviour of the voltages

- The non-isolated power converter topologies could be hazardous for the system components from safety point of view.
- PI and PR controllers provide a good response in terms of steady state error reduction, yet they experience some disturbances due to switching harmonics resulting in reduction of THD.

Based on the shortcomings listed above, the contributions of the research are summarized below:-

- Efficient dual active bidirectional DC–DC converter is employed for energy storage system. This ensures efficient high power transfer capability with low filter requirement.

- Anti windup based modified high pass filtering approach is employed to suppress the impact of high frequency transients on the DC-link capacitor. The proposed current sharing scheme is designed such that the rate of discharge/charge is limited during sudden power transients.
- Model predictive strategy has been adopted and employed to achieve reliable energy management control.
- Bode magnitude-frequency loop shaping approach is employed to design the current controllers for grid connected distribution system. Eventually, the harmonic content is reduced to achieve a better power quality.

Research works related to the control of solar photovoltaic based AC–DC type microgrid are largely focussed



on improving the power quality of the current injected to the grid or to the loads. The role of power electronics converter in microgrid is gradually advancing towards increasing the efficiency, safety and reliability of the system particularly in high power applications. In view of this, full bridge isolated DC–DC converter not only provides efficient operation but also provides galvanic isolation. Moreover, the filter requirement for PV based full bridge isolated DC–DC converter is reduced compared to conventional buck and boost topologies. Similarly, a more efficient dual active bidirectional DC–DC converter is employed for energy storage system. This topology provides a benefit over conventional bidirectional converter in terms of high power transfer capability, efficiency and low filter requirement [22].

Modified high pass filtering approach is employed to suppress the impact of high frequency transients on the DC-link Capacitor. Proposed current sharing scheme considers the thermal limits of the battery to limit current through it. It ensures battery's state of health for long term. Battery state of health is highly correlated to its operating state. Battery's operating state is characterized by the instantaneous battery voltage, state of charge, charging/discharging current rate (di/dt) and the temperature. frequency of discharge/charge cycles. Any deviation of these key parameters from allowable range could lead to degradation of the cells [23]. Hence, the proposed current sharing scheme is designed such that the rate of discharge/charge is limited during sudden power transients [24]. Eventually, the residual power is being supplied by the supercapacitor modules. In a grid connected DG environment, the power quality of the grid current and voltage is of major importance. Hence, a bode magnitude-frequency

loop shaping approach is employed to compensate for the harmonics present in the AC side of the system.

2 Hybrid AC–DC Microgrid Architecture

In this research work, a 0.5 MW solar based grid distributed generation system with dual energy storage option has been carried out. Solar based DG along with battery and supercapacitor storage is connected to the power grid through a switch at the point of common coupling. Additionally, DC loads are connected at the medium voltage DC link to form a hybrid AC–DC microgrid. The architecture of hybrid AC–DC microgrid is schematically shown in Fig. 1. To demonstrate the widely adopted distributed structure of solar photovoltaic system, two parallel PV strings comprising of 10×100 PV panels are connected to the 1kV medium voltage DC link through two individual isolated full bridge DC/DC converter. The distributed structure of solar PV panels are practically adopted to minimize any voltage/current stress on the semiconductor switches while processing and controlling high power. Energy storage solution in the form of Li-ion battery bank and supercapacitor is considered to absorb the intermittency of the solar PV output. Battery bank act as a energy buffer i.e discharges under deficit power situation while charges under excess power situation. DC link voltage profile may experience frequent short duration transients during sudden load switching or grid connection. Supercapacitor modules eventually improves the transient performance of the system because of their high power density. A better DC link voltage regulation can be achieved by incorporating fast charging and discharging feature of the

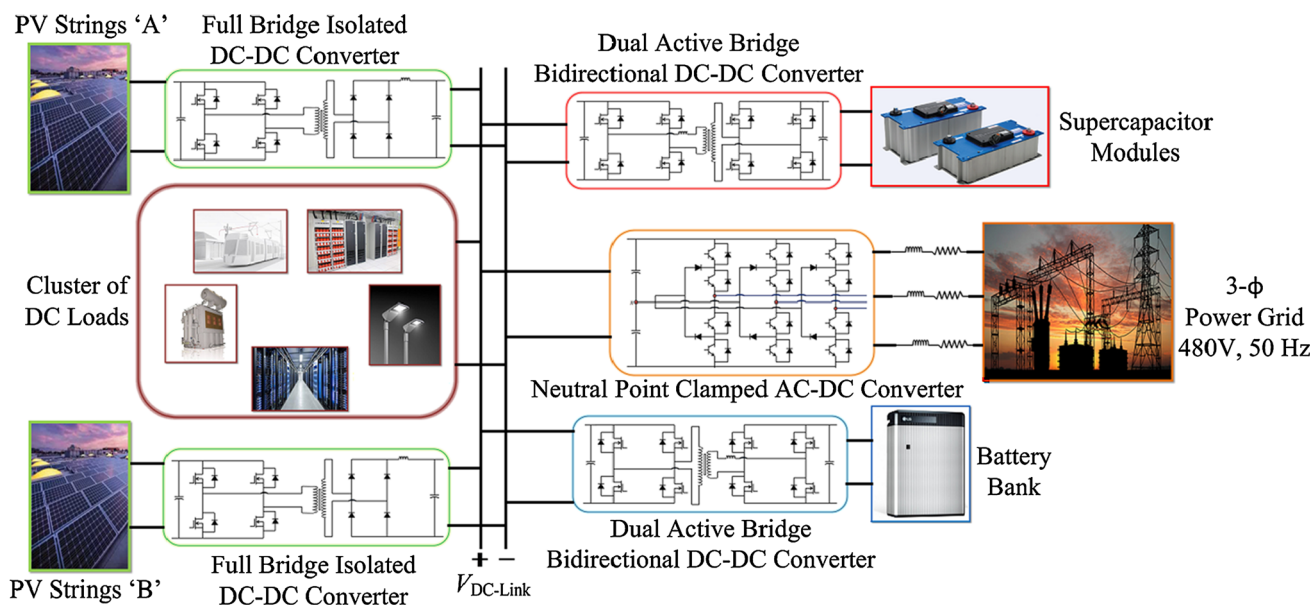


Fig. 1 System architecture of hybrid AC–DC microgrid connected to the main grid

supercapacitor. Battery bank and supercapacitors are connected to the medium voltage DC link through individual dual active bridge DC/DC converter. The hybrid AC/DC micro-grid is connected to the 480 V, 50 Hz distribution level power grid through a voltage source converter to enable active and reactive power exchange between DC link and power grid.

3 Modelling of Full Bridge Isolated DC–DC Converter for PV Applications

To model a full bridge isolated DC–DC converter for PV applications as shown in Fig. 2, we need to understand the dynamic behaviour of the converter. The input capacitance C_{in} plays a vital role in suppressing the voltage ripple at input of the DC–DC converter. Thus, it ensures stable maximum power point tracking even during switching transitions. Based on average switching action of S_{i1} and S_{i4} or S_{i2} and S_{i3} over one time period, the dynamics of the converter can be explained through (1) and (2) [25].

$$\frac{di_{iL1}}{dt} = \frac{1}{L_{i1}} (d_i \cdot n \cdot v_{PV_i} - v_{DC-link}) \tag{1}$$

$$\frac{dv_{PV_i}}{dt} = \frac{1}{C_{i1}} (i_{PV_i} - n \cdot i_{iL1}) \tag{2}$$

I_{iL} and V_{pv} are considered as the two state variables while the instantaneous duty ratio is the control variable. The state space representation of PV based isolated full bridge DC–DC

converter connected to the DC link can expressed in matrix form as:

$$\begin{bmatrix} \tilde{i}_{iL1} \\ \tilde{v}_{PV_i} \end{bmatrix} = \begin{bmatrix} A_1 & A_2 \\ A_3 & A_4 \end{bmatrix} \begin{bmatrix} \tilde{i}_{iL1} \\ \tilde{v}_{PV_i} \end{bmatrix} + \begin{bmatrix} B_1 \\ B_2 \end{bmatrix} \tilde{d}_i \tag{3}$$

Where,

$$A_1 = 0, A_2 = \frac{n \cdot D_i}{L_{i1}}, A_3 = \frac{-n \cdot D_i}{C_{i1}}, A_4 = \frac{1}{r_{PV_i} \cdot C_{i1}} \tag{4}$$

$$B_1 = \frac{n \cdot V_{PV_i}}{L_{i1}} \text{ and } B_2 = \frac{-n \cdot I_{iL1}}{C_{i1}} \tag{5}$$

The value of leakage inductance and input capacitance are chosen according to (6) and (7) in order to limit maximum peak to peak ripple in the inductor current and capacitor voltage within the specified allowable range. In our analysis, the peak to peak ripple in I_1 and V_C are limited to 5% of the rated PV current and 2% of rated PV voltage respectively.

$$L_{i1} = \frac{V_{DC-link} \cdot (1 - D_i)}{\Delta I_L \cdot f_{DAB}} \tag{6}$$

$$C_{i1} = \frac{I_{MPP_i} \cdot (1 - D_i)}{\Delta V_{PV} \cdot f_{DAB}} \tag{7}$$

The effect of varying duty ratio on PV voltage profile can be explained through state space representation and can be mathematically expressed by the transfer function G_{PV}

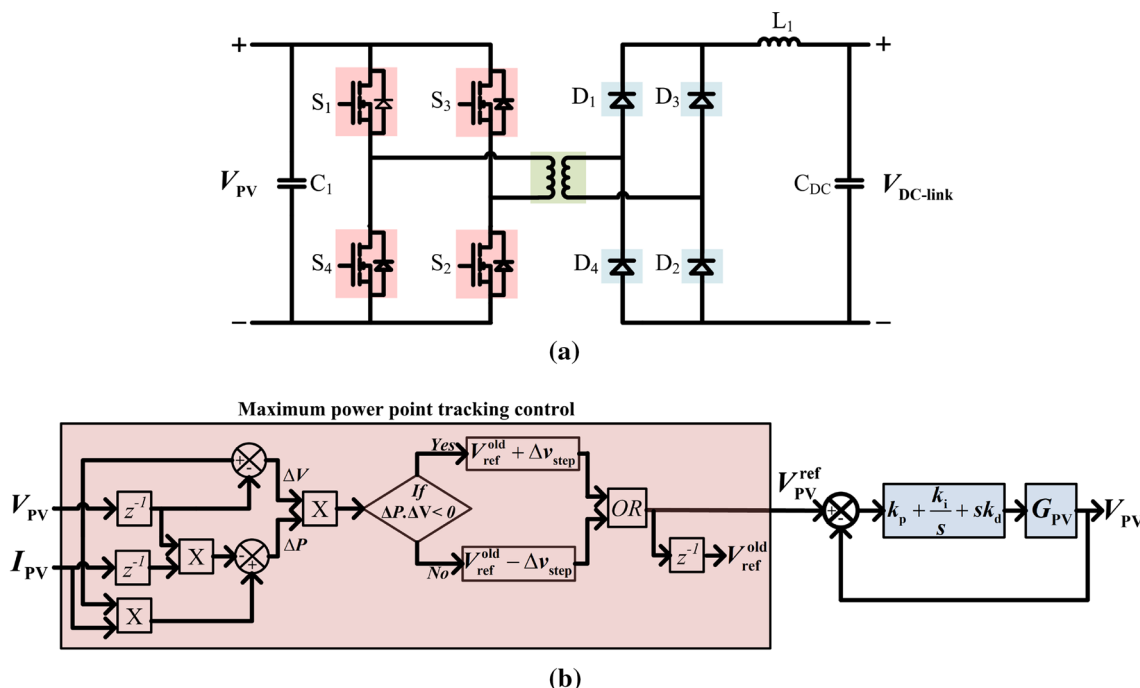


Fig. 2 a Model of a full bridge isolated DC–DC converter connected to PV strings ‘A’ b Closed loop control architecture employing MPPT and PID controller

given in (8) [25–27]. The equation suggests that the output variable i.e. PV string voltage shows a second order response when disturbances occur due to the control variable i.e. the duty ratio. This information is useful in determining the operating frequency for the MPPT controller.

$$G_{PV} = \frac{\hat{v}_{PV_i}(s)}{\hat{d}_i(s)} = \frac{\left(\frac{-n \cdot I_{l1}}{C_{i1}}\right) s + \left(\frac{-n^2 \cdot D_i \cdot V_{PV_i}}{C_{i1} \cdot L_{i1}}\right)}{s^2 - s \left(\frac{1}{r_{PV_i} \cdot C_{i1}}\right) + \left(\frac{n^2 \cdot D_i^2}{C_{i1} \cdot L_{i1}}\right)} \quad (8)$$

Small signal model of full bridge isolated DC–DC converter represented by (8) can be obtained by solving equation (A.13) and (A.14) explained in A. D represents duty ratio at steady state and n is the number of turns of the high frequency transformer. L_{i1} and L_{i1} represents the leakage inductance and input capacitance of the i^{th} PV converter. r_{PV_i} represents the dynamic resistance of the i^{th} PV String and $r_{PV_i} = \frac{v_{PV_i}}{i_{PV_i}}$.

Mitsubishi Electrical MLU series (PV-MLU250HC) PV panels are considered for the analysis. Important electrical parameters obtained from the manufacturers datasheet were utilized to accurately estimate output characteristics curve at different environmental conditions [28]. Two PV strings each composed of 10×200 PV panels having a maximum power rating of 500 kW are connected to the common medium voltage DC link through two individual isolated full bridge DC–DC converter. Each isolated DC–DC converter is controlled in such a manner that maximum power is processed through each PV string at varying environmental conditions. However, practically in a distributed type PV system architecture, different PV string may operate at different radiation and temperature level due to shading of PV panels, thermal and cooling management issues. Each PV string generates a maximum power of 500 kW operating at 310 V (PV String MPP voltage) and 1.6 kA (PV string MPP current) under standard test conditions.

The open loop performance of the full bridge DC–DC converter on the output PV voltage profile due to step disturbance in duty ratio can be graphically observed in Fig. 3 which confirms that the PV strings connected to the medium voltage DC bus behaves as a second order system oscillating at undamped frequency 8.034×10^3 and the damping ratio 0.1815 as suggested by (12). Output PV string voltage get settles to the new steady state value within 2.8 msec after the step disturbances in the duty ratio of the full bridge DC–DC Converter. The solar radiation and ambient temperature are continuously varying in nature which tends to shift the operating point of the PV panels and possibly may restrict the maximum power capability of the distributed PV system. Hence, a closed loop control architecture is employed as shown in Fig. 2b in order to extract maximum power from the PV Panels at different operating conditions by regulating either the PV current or the PV voltage using a MPPT con-

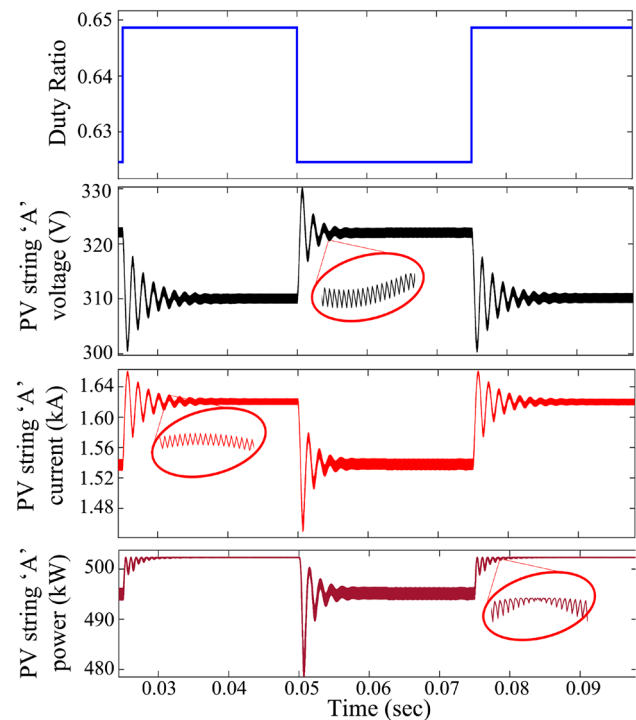
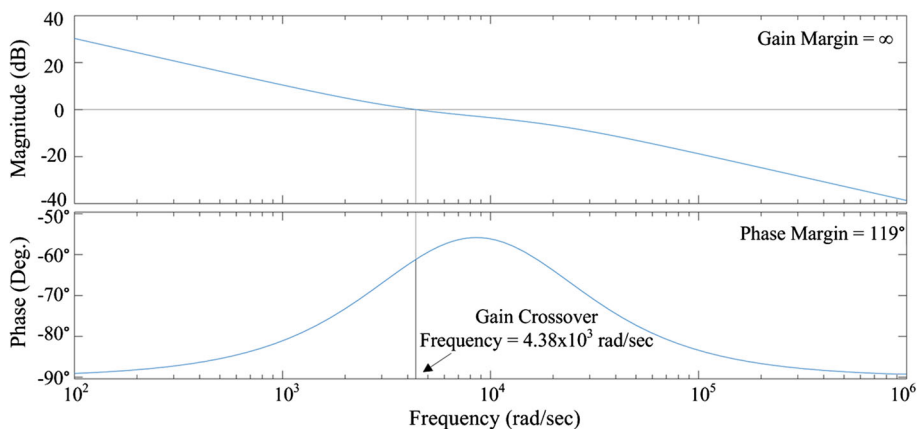


Fig. 3 Open loop response of PV string ‘A’ voltage , current and power profile due to step increase in duty ratio of a full bridge isolated DC–DC converter

troller. However, the regulation of PV output current is much complex as the level of solar radiation changes significantly during sunlight hours and thus, the operating range of the PV output current is significantly wider. On the contrary, the operating range of the output PV voltage is comparably narrower under varying irradiation levels. Only marginal change is observed in PV output voltage operating point under different temperature and irradiance levels. Hence, the regulation of the output PV voltage is achieved by incorporating a MPPT and PID based controller in the control architecture. Based on the operating environmental conditions, the maximum power point tracking (MPPT) controller generates a reference PV output voltage signal corresponding to the maximum power operating point. For a successful MPPT operation, voltage across the PV strings and the current through the PV strings are sensed at the PV strings output terminal. The MPPT algorithm then calculates the change in voltage (ΔV) and power (ΔP). The reference voltage (V_{PV}^{ref}) is obtained based on the logical criteria listed below:

- If the product ($\Delta P \Delta V$) is greater than zero, V_{PV}^{ref} is increased by Δv_{step} .
- If the product ($\Delta P \Delta V$) is less than zero, V_{PV}^{ref} is decreased by Δv_{step} .
- If the product ($\Delta P \Delta V$) is equal than zero, V_{PV}^{ref} remains unchanged.

Fig. 4 Magnitude and phase plot of compensated open loop gain for a full bridge isolated DC–DC converter connected to PV string ‘A’



The error obtained on comparing the actual and reference PV output voltage is compensated through a PID controller to generate the operating duty ratio for the converter. Finally, the PWM generator modulates the duty ratio to control the switching action of the full bridge isolated DC–DC converter.

PID controller is properly designed to improve the closed loop performance of the system. The coefficients k_p , k_i and k_d are chosen such that

- The overall closed loop transfer function is expected to be of form $1/(as+1)$ i.e a first order system with time constant ‘a’.
- Time constant is chosen such that closed loop response is 8-10 times faster than than uncompensated open loop response i.e.

$$a = \frac{1}{8 \cdot \xi \cdot \omega_n} \tag{9}$$

- The closed loop system should have adequate gain and phase margins.

Based on above performance characteristics, the tuning of PID controller is performed using MATLAB SISO Tool. The obtained optimal values of k_p , k_i , k_d is used to determine the compensated loop gain and the overall transfer function of the closed loop system. Figure 4 shows the frequency response of compensated open loop gain which confirms the stability of the closed loop system.

4 Modelling of Dual Active Bridge Bidirectional DC–DC Converter for Energy Storage Applications

The energy storage elements act as energy buffers for the microgrid especially under islanded mode of operation. Wide scale utilization of solar photovoltaic based DGs will essentially require cost effective and efficient energy storage

technologies to support the grid even if there is inadequate power supply from the PV side [29]. In our research , we have considered the Li-ion batteries and the supercapacitors for dual energy storage options in a AC–DC microgrid. In case of a medium voltage DC link operation, supercapacitors provide a fast transient response towards sudden change in load conditions especially under short duration transient peaks [30]. Hence , these can be considered as a transient surge absorbers. These short duration power transient adversely effects the dynamics of the DC link. Consequently, ripples in DC link voltage may contribute to voltage stress on grid side converter or DC–DC converter switches. Power electronic interface between the DC bus and the energy storage elements should be appropriately designed such that bidirectional flow of power/current is achieved. In order to enable co-ordinated charging and discharging of energy storage elements, a dual active bridge DC–DC bidirectional converter is employed in this research.

Dual active bridge DC–DC bidirectional converter consists of two active bridges connected through a high frequency transformer as shown in Fig. 5. All the switches operate at 50% duty cycle. Due to the switching operation of two active bridges, symmetrical square waveform is obtained at the primary and secondary terminal of the transformer. The

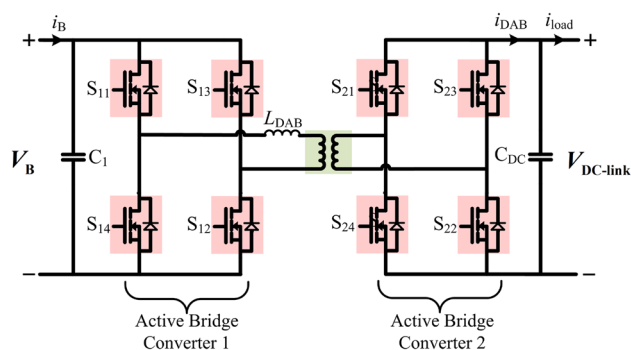


Fig. 5 A dual active bridge bidirectional DC–DC converter for Energy storage system

bidirectional exchange of the power between the DC bus and the energy storage element is dependent on the phase lag or lead between the two signals. The dynamics of the dual active bridge bidirectional DC–DC converter can be explained through (10). The steady state power flow can be estimated through (11).

$$\frac{di_{LB}}{dt} = \frac{1}{L_{BDAB}} \int (V_p - V_s).dt \tag{10}$$

$$P_{bat} = \frac{V_B \cdot V_{DC-Link} \cdot \phi \cdot (\pi - \phi)}{\pi \cdot \omega \cdot n \cdot L_{BDAB}} \tag{11}$$

Maximum power exchange (either during charging or discharging) can be achieved for a phase difference of $\phi = 90^\circ$. For rated/maximum capacity of a battery or a supercapacitor, the value of coupling inductor can be chosen for a particular value of switching frequency f_{DAB} and maximum power rating $P_{B_{rated}}$ according to (12).

$$L_{BDAB} \leq \frac{V_B \cdot V_{DC-Link}}{8 \cdot f_s \cdot n \cdot P_{bat_{rated}}} \tag{12}$$

LG Chem 48V, 126 Ah RESU 6.5 Li-ion battery pack is considered for the analysis [31]. The technical specification of the battery pack is extracted from the manufacturer datasheet to construct the equivalent thevenin’s model of Li-ion battery . A battery bank consisting of 100 LG Chem batteries in parallel is connected to the medium voltage DC bus through a dual active bridge bidirectional DC–DC converter to ensure proper charging and discharging. At a steady state value of $\phi = 45^\circ$, 187.5 kW power can be discharged through the battery bank. The energy storage system should be adequately designed to deliver or absorb power so as to achieve proper DC-link voltage regulation. Hence it becomes important to understand the behaviour of DC link voltage profile during charging and discharging of battery bank/supercapacitor through the bidirectional converter. The dynamics of the DC link connected to battery through a bidirectional converter can be explained through (14).

$$C_{DC} \frac{dv_{DC-link}}{dt} = i_{BDAB} - i_{Load} \tag{13}$$

$$C_{DC} \frac{dv_{DC-link}}{dt} = \frac{P_{bat}}{V_{DC}} - \frac{v_{DC-link}}{R_{Load}} \tag{14}$$

C_{DC} represents the capacitance of the DC bus. i_{Load} is introduced to examine the effect of variation of load on the DC bus. From our application point of view, i_{Load} represents deficit or excess power based on loading conditions. R_{Load} represents the load resistance as seen by the DC bus. According to the operating principle of dual active bridge bidirectional DC–DC converter, the power delivered

(or absorbed) by the battery is dependent on the phase difference between the switching states of two active bridges. Hence, the dynamics of the DC link can be studied through analysing the impact of variation of phase difference ϕ on the DC link voltage.

Considering, $V_{DC-link}$ as the state variable and ϕ as the control variable, the small signal dynamics (in s-domain) is represented by linearizing equation (14) as

$$G_{DAB} = \frac{v_{DC-link}(s)}{\phi(s)} = \frac{k_{DAB}}{(s \cdot \tau_{DAB} + 1)} \tag{15}$$

where, $k_{DAB} = \frac{R_{Load} \cdot V_B}{\omega \cdot n \cdot \pi \cdot L_{BDAB}} \left(1 - \frac{2\phi}{\pi}\right)$ and $\tau_{DAB} = R_{Load} \cdot C_{DC}$ (16)

(17)

Open loop transfer function G_{DAB} suggests that the dual active bridge bidirectional DC–DC converter connected to the battery bank/supercapcitor can be considered as a first order system with DC gain as k_{DAB} and time constant as τ_{DAB} . The DC gain is dependent on the steady state value of phase difference while the time constant is dependent on the load resistance R_{Load} . A step increase in load resistance results in slower transient response as the value of time constant increases. The effect on DC link voltage profile due to step variations ($\pm 5\%$ around steady state value of $\phi=0.7854$ rad) in phase difference ϕ is shown in Fig. 6. It shows that the DC link voltage instantaneously oscillates around the steady state value of 1 kV during load variation (due to variation in ϕ). It can be concluded that a closed loop architecture needs to be adopted to regulate the DC link voltage at a constant value of 1 kV and to improve the transient response of the system which is discussed in the next section, battery bank and supercapacitor based dual energy storage system connected

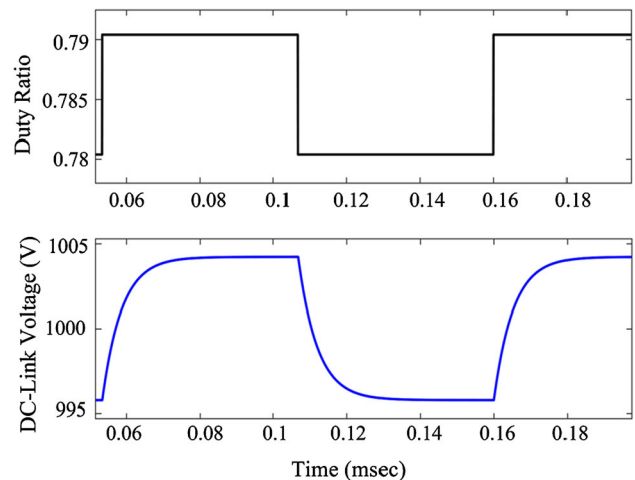


Fig. 6 Impact of step variation in phase difference (ϕ) on the DC link voltage profile

to the medium voltage DC link through dual active bridge bidirectional converter serves the following objectives:

- Acts as energy buffer
- Provides effective regulation of medium voltage DC link

5 DC-Link Voltage Regulation

The common DC link is an important element of an AC–DC microgrid which maintains the power balance between AC and DC side of the microgrid. The dynamics of the DC link provides an insight on the stability of the DC link voltage due to power imbalance at the DC link terminals. The dynamics at the DC link terminal can be explained using (18)

$$C_{DC} \frac{dv_{DC-link}}{dt} = \frac{P_{ESS} - P_{net}}{V_{DC-link}} \tag{18}$$

Where $P_{ESS}=P_{bat}+P_{SC}$ is the power supplied or absorbed by the dual energy storage system and $P_{net}=P_{PV}-P_{DC}-P_{3\phi}$ is the deficit or excess power seen by the high voltage DC link in absence of any storage system. Energy storage in the form of battery bank and supercapacitor is adopted not only to balance the power flow at the DC link terminals but also to regulate the DC link voltage. Under steady state condition, the term $P_{ESS}-P_{net}$ has a infinitely small value and does not effect the DC link voltage profile. However, DC link voltage may be subjected to short duration transients at the instant of load switching or grid connection/disconnection. Practically, battery causes a delay equal to 4 times $R_{Bat} \cdot C_{Bat}$ during charging and discharging due to internal resistances and capacitance and hence produces short duration transients on DC link. In high power applications, the intermittent nature of the solar PV output also affects the thermal management of the battery.

Hence, a supercapacitor is employed along with the battery bank to suppress the high frequency short duration transient. Supercapacitors have high energy density and can absorb these transients due to their fast charging and discharging ability. Supercapacitor also plays important role

in improving the thermal management of the battery. To achieve this, a current sharing scheme is adopted by the energy management controller described in section to obtain the reference current for both supercapacitor and battery bank such that the thermal limits of the battery is prevented.

The transfer function G_{DAB} and uncompensated open loop response suggests that a closed loop feedback control needs to be designed to improve the transient performance and to regulate the high voltage DC link. A proportional integral controller is employed in closed loop control architecture as shown in Fig. 7. The closed loop system is designed such that compensated plant should be 10 times faster than the original plant. Accordingly, the closed loop transfer function of the dual active bridge bidirectional DC–DC converter including a PI controller can be written as:-

$$C_{DAB} = \frac{G_{DAB} \cdot G_{PI}}{1 + G_{DAB} \cdot G_{PI}} \tag{19}$$

where, $G_{PI} = \left(k_{p1} + \frac{k_{i1}}{s} \right)$ (20)

The coefficients k_{p1} and k_{i1} are chosen such that:-

- The overall closed loop transfer function is expected to of the form $1/(\tau_{des} \cdot s+1)$ which represents a single order system.
- The closed loop response should be faster than the uncompensated open loop response and hence τ_{des} chosen to be 1/10th of τ_{DAB} i.e.

$$\tau_{des} = \frac{\tau_{DAB}}{10} \tag{21}$$

According the above mentioned conditions, the values of k_{p1} and k_{i1} are calculated using (22).

$$k_{p1} = \frac{\tau_{DAB}}{k_{DAB} \cdot \tau_{des}} \text{ and } k_{i1} = \frac{1}{k_{DAB} \cdot \tau_{des}} \tag{22}$$

The closed loop response of the battery bank connected to the high voltage DC link through a compensated dual active

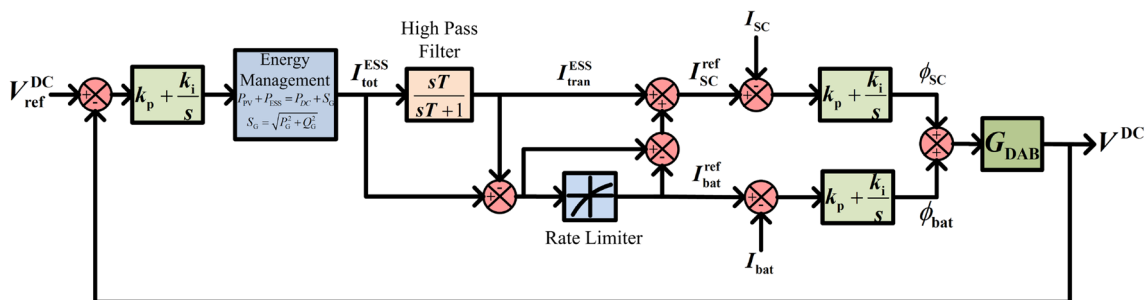


Fig. 7 Closed loop architecture for proper DC voltage regulation

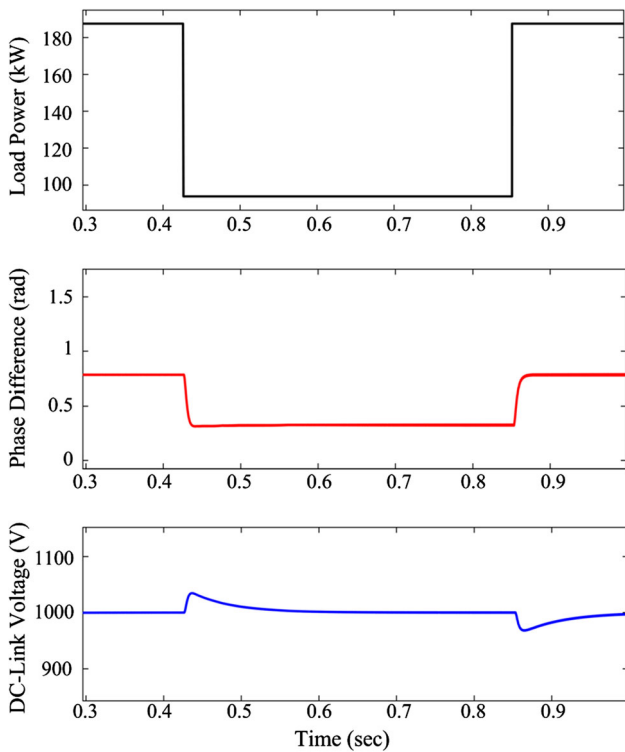


Fig. 8 Closed loop response of DC-link voltage due to step changes in DC load

bridge bidirectional DC–DC converter is shown in Fig. 8. It can be seen that DC link voltage is regulated at 1 kV on step variations in load power.

6 Energy Management of Hybrid DC–AC Microgrid

Energy management is a core section that plans, organizes, coordinates and monitors the system parameters, power utility information, services and energy resources based on the techno-economical constraints imposed on the system. System uncertainties such as intermittent PV power output due to varying environmental conditions, sudden active and reactive support to the three phase utility grid, transient power surges at DC load, islanding of microgrid etc. need to be considered to define the stable operation of the AC–DC microgrid. Energy management section performs the following functions:

- Exchange of power to or from the utility grid
- Economic operation of microgrids
- Optimal scheduling of required power among different energy resources
- Load shedding (in worst case scenario)
- Dispatch of power to the local critical loads

In order to achieve cost effective operation of AC–DC microgrid, PV based DC–DC converters are operated to ensure maximum power extraction from the distributed PV System. Batteries act as energy buffer to absorb and supply excess power and deficit power respectively based on the grid and critical DC load requirement. The charging and discharging capacity of Li-ion batteries are limited within range $[SOC_{max}, SOC_{min}]$ to prevent battery degradation and thermal limits. Usually, operating capacity of a battery is limited between 30–70% of the maximum capacity for efficient, economical and durable operation of Li–ion batteries. Super-capacitor comes into operation when a high frequency short duration transient is experienced by the DC link. Although both battery and grid can act as a energy buffer yet wide scale penetration of intermittent renewable resources may disturb the inertia of the whole power system. Additionally, Li–ion batteries shows slow response towards sudden transient variation in load power which introduces ripple in the DC link voltage profile.

The energy management controller decides the reference operating power for the dual energy storage system, active and reactive power supplied to the grid based on four cases considering the effect of stochastic response of PV power, battery state of charge and power demand by the DC loads.

Case 1:- If the sum of grid power requirement and the DC load requirement exceeds the generated PV power, grid requires only active power

- if $SOC_{min} \leq SOC_{bat}(t) \leq SOC_{max}$

$$P_{PV}(t) + P_{ESS}^{dis} = P_{grid}(t) + P_{DC}(t) \tag{23}$$

- if $SOC_{bat}(t) \leq SOC_{min}$

$$P_{PV}(t) = P'_{grid}(t) + P_{DC}(t) \tag{24}$$

$$P_{grid}^*(t) \rightarrow P_{PV}(t) - P_{DC}(t) \tag{25}$$

Case 2:- If the sum of grid power requirement and the DC load requirement exceeds the generated PV power, grid requires both active and reactive power

- if $SOC_{min} \leq SOC_{bat}(t) \leq SOC_{max}$

$$P_{PV}(t) + P_{ESS}^{dis} = |S_{grid}(t)| + P_{DC}(t) \tag{26}$$

- if $SOC_{bat}(t) \leq SOC_{min}$

$$P_{PV}(t) = |S'_{grid}(t)| + P_{DC}(t) \tag{27}$$

$$P_{grid}^*(t) \rightarrow \sqrt{(P_{PV}(t) - P_{DC}(t))^2 + (Q_{grid}^*)^2} \tag{28}$$

Case 3:- If the generated PV power exceeds the sum of grid and DC load power requirement, grid requires only active power.

- if $SOC_{min} \leq SOC_{bat}(t) \leq SOC_{max}$

$$P_{PV}(t) = P_{ESS}^{ch}(t) + P_{grid}(t) + P_{DC}(t) \tag{29}$$

- $SOC_{bat}(t) \geq SOC_{max}$

$$P_{PV}(t) = P'_{grid}(t) + P_{DC}(t) \tag{30}$$

$$P^*_{grid}(t) \rightarrow P_{PV}(t) - P_{DC}(t) \tag{31}$$

Case 4:- If the generated PV power exceeds the sum of grid and DC load power requirement, grid requires both active and reactive power.

- if $SOC_{min} \leq SOC_{bat}(t) \leq SOC_{max}$

$$P_{PV}(t) = P_{ESS}^{ch}(t) + |S_{grid}(t)| + P_{DC}(t) \tag{32}$$

- if $SOC_{bat}(t) \leq SOC_{min}$

$$P_{PV}(t) = |S'_{grid}(t)| + P_{DC}(t) \tag{33}$$

$$P^*_{grid}(t) \rightarrow \sqrt{(P_{PV}(t) - P_{DC}(t))^2 + (Q^*_{grid})^2} \tag{34}$$

Based on above cases, energy management control can be achieved through model predictive control. Model predictive controller allows optimal power balance and control in a multi generation distributed energy system through a robust and stochastic formulation. It enables us to predict the system output response by minimizing the cost function over discrete control horizon. The cost function comprises of:

- Weighted sum of PV power ($\alpha_{PV} P_{PV}$), battery power ($\alpha_B P_B$), supercapacitor power ($\alpha_{SC} P_{SC}$) and grid power ($\alpha_g P_{grid}$) for optimal resource allocation.
- Weighted sum of battery ($\beta_B \Delta P_B$) and supercapacitor power ($\beta_{SC} \Delta P_{SC}$) deviation for rate limitation and coordinated action of energy storage system.
- Penalty term ($\gamma_{DC} (V_{DC}(t + 1) - V_{DC}(t))$) for any deviation in DC voltage to achieve efficient DC voltage regulation.

The objective of model predictive based energy management controller is to estimate the next state of the decision variables through minimization of cost function over n_c control horizon. The charging/discharging reference current through the battery bank and supercapacitor modules is optimally determined depending on the loading conditions, grid

status, maximum power through PV strings and state of charge constraints.

$$\sum_{i=1}^2 P_{PV}(t) + \sum_{i=1}^{n_b} P_B(t) + \sum_{i=1}^{n_{sc}} P_{SC}(t) - S_{grid}(t) - \sum_{i=1}^{n_{load}} P_{load}(t) = P_{net} \tag{35}$$

$$x(t) = \left[\sum_{i=1}^{n_b} P_B(t) \sum_{i=1}^{n_{sc}} P_{SC}(t) \right] \tag{36}$$

$$u(t) = \left[S_{grid}(t) \sum_{i=1}^{n_{load}} P_{load}(t) SOC_B(t) \right] \tag{37}$$

$$d(t) = P_{net}(t) \tag{38}$$

$$P_B(t + 1) = P_B(t) + \sum_{i=1}^2 P_{PV}(t) - S_{grid}(t) - \sum_{i=1}^{n_{load}} P_{load}(t) \tag{39}$$

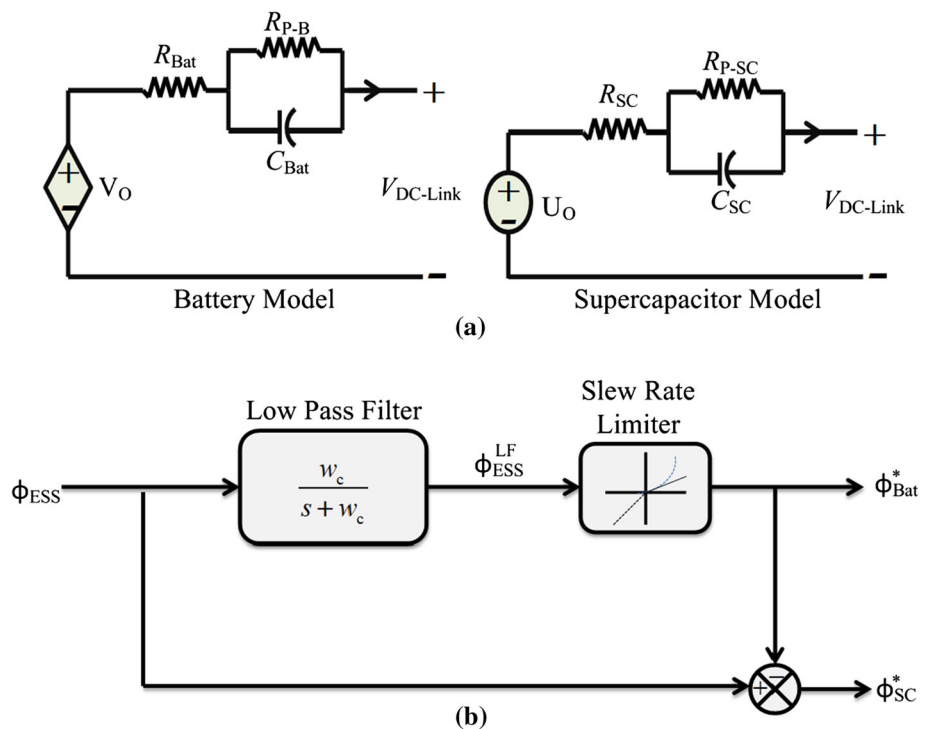
$$P_{SC}(t + 1) = P_{SC}(t) + \sum_{i=1}^2 P_{PV}(t) - S_{grid}(t) - \sum_{i=1}^{n_{load}} P_{load}(t) \tag{40}$$

For an optimal response, the reference for the supercapacitor and battery bank can be estimated by minimizing the cost function as given below:

$$J = \left(\begin{array}{l} \sum_{i=1}^{n_c} \alpha_{PV} P_{PV}(t + i) + \alpha_B P_B(t + i) + \\ \alpha_{SC} P_{SC}(t + i) + \alpha_g P_{grid}(t + i) + \\ \sum_{i=1}^{n_c} \beta_B \Delta P_B(t + i) + \beta_{SC} \Delta P_{SC}(t + i) + \\ \sum_{i=1}^{n_c} \gamma_{DC} (V_{DC}(t + i) - V_{DC}(t + i - 1)) \end{array} \right) \tag{41}$$

Further, the current sharing between the supercapacitor and the Li-ion battery is based on the concept of decomposition of total ESS charging/discharging current into high frequency and low frequency components. The electrical equivalent thevenin’s model of battery and supercapacitor is shown in Fig. 9a. In a dual active bridge bidirectional DC–DC converter, power is related to the phase difference between (ϕ) switching of individual bridges. Accordingly, the control variable in this application is ϕ which is proportional to the battery power and current as suggested in the equation (15). Thus, power sharing among the battery bank and supercapacitor is based on decomposition of ϕ_{ESS} into low frequency component and high frequency transients. A high pass filter is used to extract the low frequency components

Fig. 9 **a** Equivalent thevenin’s model of battery and supercapacitor, **b** Power sharing scheme for battery bank and supercapacitor modules



of ϕ_{ESS} whose cutoff frequency is chosen between 5–10 Hz. High frequency transients thus obtained are taken care of by the supercapacitor. In high power applications, due to variable nature of solar radiation the total battery charging/discharging current required may sometimes be very high which may test the thermal limits of the battery. In order to enhance the thermal management and the lifetime of the battery, the low frequency component of ϕ_{ESS} is passed through a slew rate limiter considering the thermal limits. As a result, battery bank charging/discharging current takes certain time to reach to the final steady state value and in the meantime, supercapacitor takes care of the transient developed on the medium voltage DC bus. The ESS power sharing scheme is shown in Fig. 9b.

7 Modelling of Neutral Point Clamped Voltage Source Converter for 3ϕ Grid Connection

‘A’ phase leg of a neutral point clamped DC–AC converter consists of two half bridges (S_{11} and S_{12} forms one while S_{21} and S_{22} forms another) as shown in Fig. 10. The DC link splits into two half at the input terminal of a NPC converter. The dynamics of the NPC converter can be mathematically explained using (42)

$$V_c = \frac{V_{DC-link}}{2} m(t) \tag{42}$$

7.1 Current Control of Grid Connected NPC AC–DC Converter

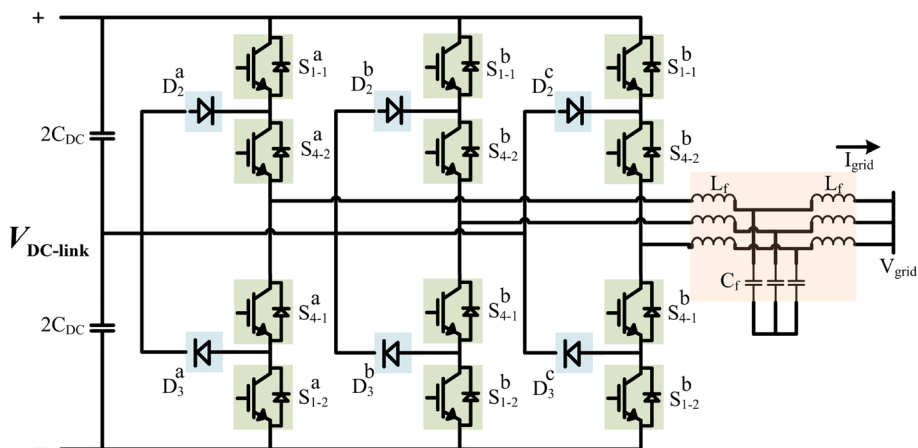
Certain standard grid requirement and codes are specified for integration of renewable based DGs. It provides a technical guideline to the network operators for planning, control and expansion of distributed generation technology. IEEE 929, UL 1741, IEEE 1547, IEC 61727 are certain relevant standards for integrating renewable based DGs into the grid [32,33]. Voltage harmonic level, voltage amplitude and frequency variations, injected current harmonic levels, total harmonic distortion are the parameters of interest while designing and evaluating the control scheme of the power converters [34]. Grid side current controller can be modelled in rotating dq frame, the stationary $\alpha\beta$ frame, and the natural abc frame.

7.2 Grid Current Control Architecture in dq Frame

In this section, synchronously rotating frame (dq) based current controllers are designed. As the grid current in abc frame gets transformed to dc values in dq reference frame, two PI controllers are employed for both d axis and q axis controller. The AC side system dynamics can be represented using (43):-

$$L_g \frac{di_{abc}}{dt} = -R_g \cdot i_{abc} + V_{c,abc} - V_{grid,abc} \tag{43}$$

Fig. 10 Schematic diagram of a neutral-point clamped DC–AC converter connected to the 3- ϕ power grid



Using Park Transformation,

$$V_{\text{grid},d} - V_{c,d} = R_g \cdot i_d + L_g \frac{di_d}{dt} - \omega \cdot L_g \cdot i_q \tag{44}$$

$$V_{\text{grid},q} - V_{c,q} = R_g \cdot i_q + L_g \frac{di_q}{dt} + \omega \cdot L_g \cdot i_d \tag{45}$$

The d axis equation (44) contains i_q term and the q axis equation (45) contains i_d term. Hence, we can say that $d - q$ axis current dynamics are cross-coupled. Two control inputs are defined as u_d and u_q which regulates the error between the reference and actual $d - q$ axis current using a PI controller. It helps in decoupling the $d - q$ axis current dynamics and hence i_d and i_q can be controlled independently as shown in the Fig. 11. The modulating signals m_d and m_q can be obtained as follows:-

$$m_d = \frac{2}{V_{\text{DC-link}}} [u_d - \omega \cdot L_g \cdot i_q + V_{\text{grid},d}] \tag{46}$$

$$m_q = \frac{2}{V_{\text{DC-link}}} [u_q + \omega \cdot L_g \cdot i_d + V_{\text{grid},q}] \tag{47}$$

Where,

$$u_d = \left(k_{p2} + \frac{k_{i2}}{s} \right) \cdot (i_d^* - i_d) \tag{48}$$

$$u_q = \left(k_{p3} + \frac{k_{i3}}{s} \right) \cdot (i_q^* - i_q) \tag{49}$$

The open loop gain G_{OC} of transfer function with i_d^* (reference d axis current) as input and i_d (actual d axis current) can be obtained from the Fig. 11.

$$G_{OC} = C_C \cdot G_{AC} = \frac{(s \cdot k_p + k_i)}{s(s \cdot L_g + R_g)} \tag{50}$$

Controller parameters k_p and k_i are designed such that the closed loop transfer function should be a first order system with desired closed loop time constant τ_{CL} . In case of

a grid connected system, τ_{CL} is chosen such that it provides a fast transient response i.e. it should be adequately small but controller bandwidth should not exceed $(1/10)^{th}$ of the switching frequency. Hence the desired closed response can be expressed as:-

$$G_{CL} = \frac{C_C \cdot G_{AC}}{1 + C_C \cdot G_{AC}} = \frac{1}{s \cdot \tau_{CL} + 1} \tag{51}$$

7.3 Grid Current Control Architecture in $\alpha\beta$ Frame

The current controller design using PI controllers in dq frame was based on improving the transient response so as to achieve the desired closed loop time constant. Total harmonic distortion is a measure of the power quality in grid current or voltage profile. THD quantifies the amount of harmonics present in the grid current/voltage based on its magnitude at different harmonic frequencies. Control architecture design using transient analysis does not take into account frequencies which might have a distortion effect on the injected grid current profile. Hence, an alternate current controller design approach is proposed based on frequency response analysis. It includes bode plot- magnitude and frequency loop shaping in order to improve the controller response based on specified design requirements. In other words, magnitude and frequencies at critical frequencies are compensated using a higher order current controller to achieve better grid current power quality. In our work, the higher order current controller is designed in $\alpha\beta$ frame.

The control architecture for $\alpha\beta$ frame is same as that of dq frame. The difference lies in the design approach. In dq frame, the three phase AC grid currents (i_{abc}) are transformed into two equivalent DC quantities (i_d, i_q). The control approach is adopted only to reduce steady state current values of i_d and i_q . However, the three phase AC grid currents (i_{abc}) in $\alpha\beta$ frame are transformed into two equivalent alternating quantities (i_{α}, i_{β}). A control strategy that involves reduction of steady state error in both magnitude and frequency domain

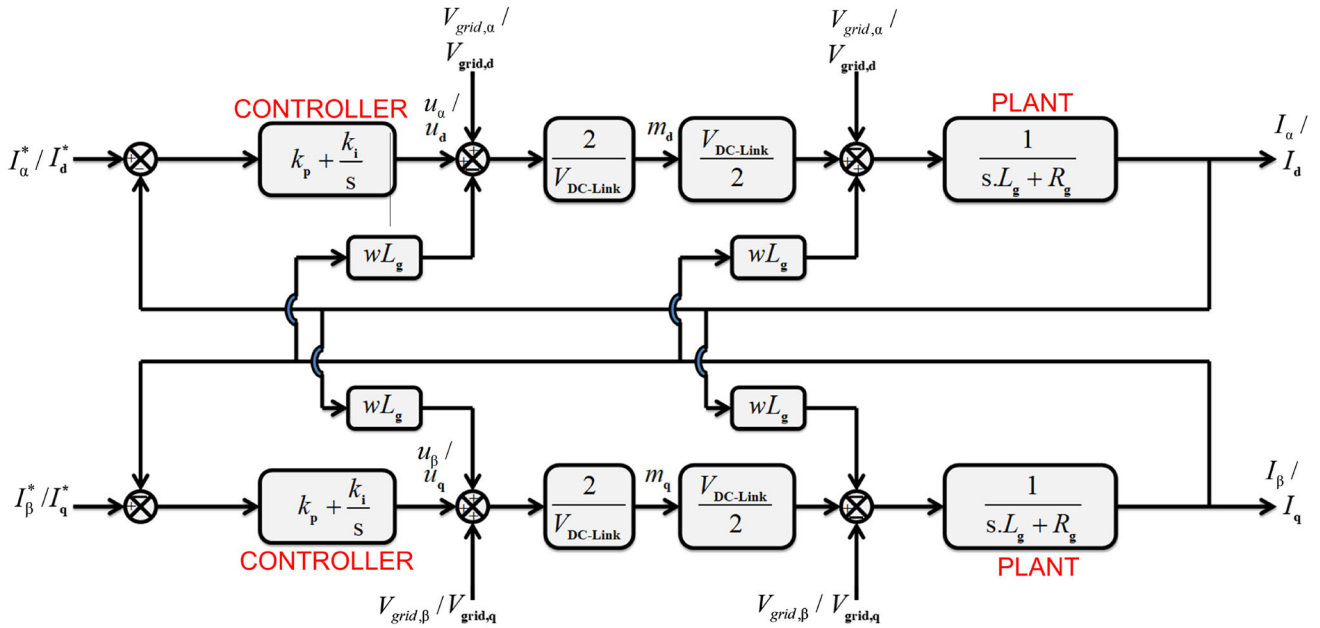


Fig. 11 Closed loop current control architecture for a grid connected neutral point clamped AC–DC converter

needs to be employed. Hence, bode loop shaping is employed to compensate for magnitude and phase at desired frequencies by including poles and zeros accordingly.

The block diagram for current control architecture in $\alpha\beta$ frame is same as that of dq frame as shown in Fig. 11. Using equation (43) and applying three phase to two phase transformation, the modulating signals m and m_{fi} are :-

$$m_\alpha = \frac{2}{V_{DC-link}} [u_\alpha - \omega.L_g.i_\beta + V_{grid,\alpha}] \tag{52}$$

$$m_\beta = \frac{2}{V_{DC-link}} [u_\beta + \omega.L_g.i_\alpha + V_{grid,\beta}] \tag{53}$$

Where,

$$u_\alpha = C_\alpha(s) \cdot (i_\alpha^* - i_\alpha) \tag{54}$$

$$u_\beta = C_\beta(s) \cdot (i_\beta^* - i_\beta) \tag{55}$$

The open loop gain G_{oc} of the compensated closed loop current control scheme can be written as:-

$$G_{OC} = C(s) \cdot \left(\frac{1}{sL_g + R_g} \right) \tag{56}$$

To achieve high gain at system operating frequency (ω_0) i.e. 50 Hz, a complex conjugate pair is included at 314 rad/sec. This ensures zero steady error in both magnitude and phase domain at the desired nominal frequency. Figure 12 shows a magnitude-frequency response of open loop gain G_{oc} including compensator $C_1(s)$ defined by:-

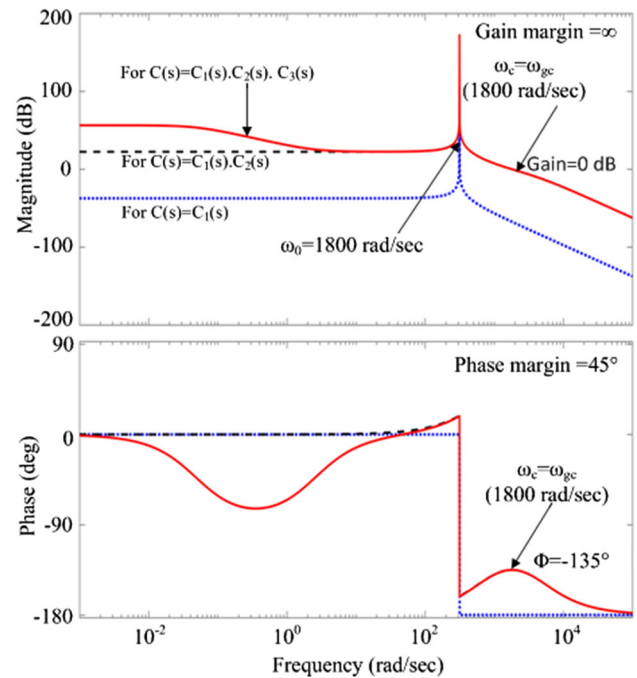


Fig. 12 Bode plot showing magnitude and frequency response of compensated open loop gain G_{oc}

$$C(s) = C_1(s) \cdot K(s) \tag{57}$$

Where,

$$C_1(s) = \frac{(s + 8.33)}{(s + 98596)}, \quad K(s) = 1 \tag{58}$$

Dotted blue curve in Fig. 12 suggests that for frequencies greater than 314 rad/sec the phase is around -180 . This corresponds to a marginally stable system or an unstable system against system variations. Phase margin at the desired critical frequency decides the stability of the system. In our work, critical frequency is chosen according to the bandwidth of the controller such that $\omega_c < \omega_b < 2\omega_c$. Accordingly, for a chosen controller bandwidth of 2700 rad/sec (9 times the operating frequency), the desired critical frequency or gain crossover frequency should be 1800 ($\omega_b/1.5$). Including a lead filter ensures adequate phase margin at the critical frequency. A gain is multiplied which guarantees 0 dB magnitude crossing at the critical frequency. The current controller $C(s)$ defined in (57) can be modified to improve the stability of the system by ensuring adequate gain and phase margin. The modified controller $C(s)$ can be written as

$$C(s) = C_1(s) \cdot C_2(s) \cdot K(s) \tag{59}$$

$$C_2(s) = 5688 \cdot \frac{(s + 745)}{(s + 4346)}, K(s) = 1 \tag{60}$$

Black dashed curve in Fig. 12 represents the frequency response of modified G_{OC} including $C_2(s)$. It can be observed that at the gain cross over frequency (1800 rad/sec) the magnitude plot crosses 0 Db gain and the phase is -135. This corresponds to a phase margin of 45 ensuring a stable system. It can also be observed that all the frequencies less than $\omega_0=314$ rad/sec have equal magnitude. This could result in propagation of high frequency noise through the controller. To avoid this, a significant gain must be added to the low frequency region (particularly close to 0).

Finally, a lag compensator is employed to improve the gain in lower frequency range. Hence the controller defined in equation (59) can be finally modified to enhance the steady state accuracy of the current controller. The final current controller $C(s)$ can be written as

$$C(s) = C_1(s) \cdot C_2(s) \cdot C_3(s) \tag{61}$$

where,

$$C_3(s) = \frac{(s + 2.5)}{(s + 0.005)} \tag{62}$$

The red curve in Fig. 12 shows the compensated frequency response of the closed loop current controller in $\alpha\beta$ frame. It can be seen the system is stable as it has sufficient phase margin and ∞ gain margin. It can also be observed from the magnitude corresponding to the switching frequency harmonics lies on -40 dB/decade slope. Dominant switching harmonic contents are reduced which results in better grid current power quality.

8 Results and Discussion

The hybrid AC–DC solar photovoltaic based microgrid with dual energy storage option shown in Fig. 1 is implemented in MATLAB Simulink environment to show the effectiveness of:-

- PV side control (MPPT)
- Grid side converter control
- Energy management controller
- DC link Regulation

The overall control structure of the hybrid AC–DC microgrid consisting of PV strings, battery bank, supercapacitor module and three phase grid is presented in the Fig. 13. DC loads are considered as constant power loads connected to the 1 kV DC link while the three phase 480 V, 50 Hz distribution level power grid is considered as the three phase load connected through a voltage source inverter. The grid side controller is designed such that both active and reactive power can be supplied to the power grid. The PV system consisting of two distributed PV strings is operated at same irradiance. The system parameters are listed in Table 2. In our research, overall control structure is divided into three segments. Primary control deals with maximum power extraction from PV string for proper utilization of solar power. Efficient power point tracking is achieved through joint action of MPPT and PID controller. Secondary control deals with reference current generation for battery bank, supercapacitor module and local distribution grid. Effective power management, optimal resource allocation and system stability is ensured through model predictive based energy management controller, PI based DC link voltage controller and high pass filtering scheme. Tertiary control deals with reference current tracking using PI based current controllers for battery bank, supercapacitor and grid converter. The values of parameters for each controller is listed in Table 3 The performance and the transient response of the proposed hybrid AC–DC microgrid under different loading scenario and varying solar radiation profile.

At time $t=0$, the microgrid is switched ON. A DC load of 400 kW is initially connected to the medium voltage DC link. The two PV strings are operated at 500 W/m^2 irradiance level while the state of charge of the battery is initially assumed to be 45% of the rated battery capacity. The microgrid is assumed to be in islanded mode initially as the switching action is blocked for the grid side converter. It can be seen from the Fig. 14a that the MPPT controller quickly responds to the operating environmental conditions and within few milliseconds maximum power is extracted from the two PV strings. Due to the energy management control design, the excess power is initially absorbed by the supercapacitor. To maintain DC link voltage at 1 kV, battery bank absorbs the

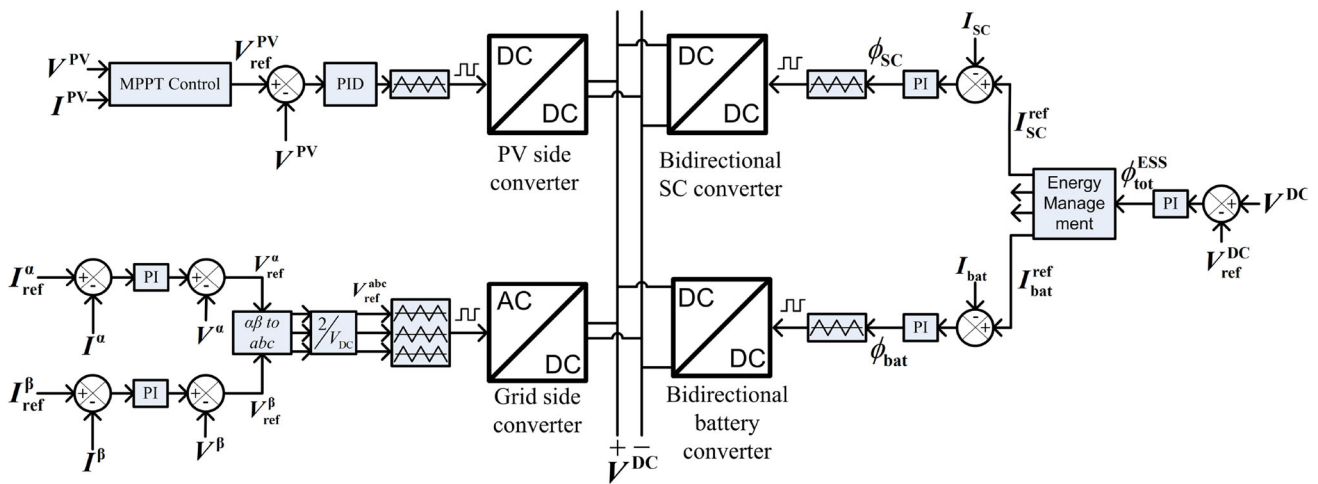


Fig. 13 Overall control architecture of converter based AC–DC microgrid

Table 2 System Parameters for operation and control solar photovoltaic based microgrid including energy storage

System parameters	Representation	Values
V_{grid}	Three phase grid voltage	$480V_{rms} (1-1)$
$V_{DC-Link} (V)$	DC-link voltage	1000 V
$C_{DC-Link} (V)$	DC-link capacitance	600 μF
P_{PV}	Rated PV Power	250 kW each
V_{MPPT}	MPPT voltage	300-310 V
f_{PV}	PV converter Switching frequency	50 kHz
L_{A1}, L_{A2}	PV converters leakage inductance	177.5 μH
C_{A1}, C_{A2}	PV converters input capacitance	927.58 μH
V_B	Nominal battery voltage	48 V
B_{Cap}	Battery capacity	126 Ah
R_g	Grid filter resistance	5 m Ω
L_g	Grid filter inductance	750 μH
L_{DAB}	Dual active bridge Coupling Inductance	0.08 μF
f_{PV}	PV converter Switching frequency	20 kHz
ω_0	System operating frequency	314 rad/sec

Table 3 Paramters of PV side, grid side, energy storage side and DC voltage controllers

Controller parameters	Value	Controller parameters	Value
PV side	k_p	Battery side	k_p
	k_i		k_i
	k_d		
SC	k_p	DC voltage	k_p
Side	k_i	Controller	k_i
dq based	k_p	$\alpha\beta$ based	K(s)
Grid side	k_i	Grid side	$\frac{5688s^3+4.3 \times 10^6s^2+4.6 \times 10^7s+8.27 \times 10^7}{s^3+1.02 \times 10^5s^2+4.29 \times 10^8s+2.14 \times 10^6}$

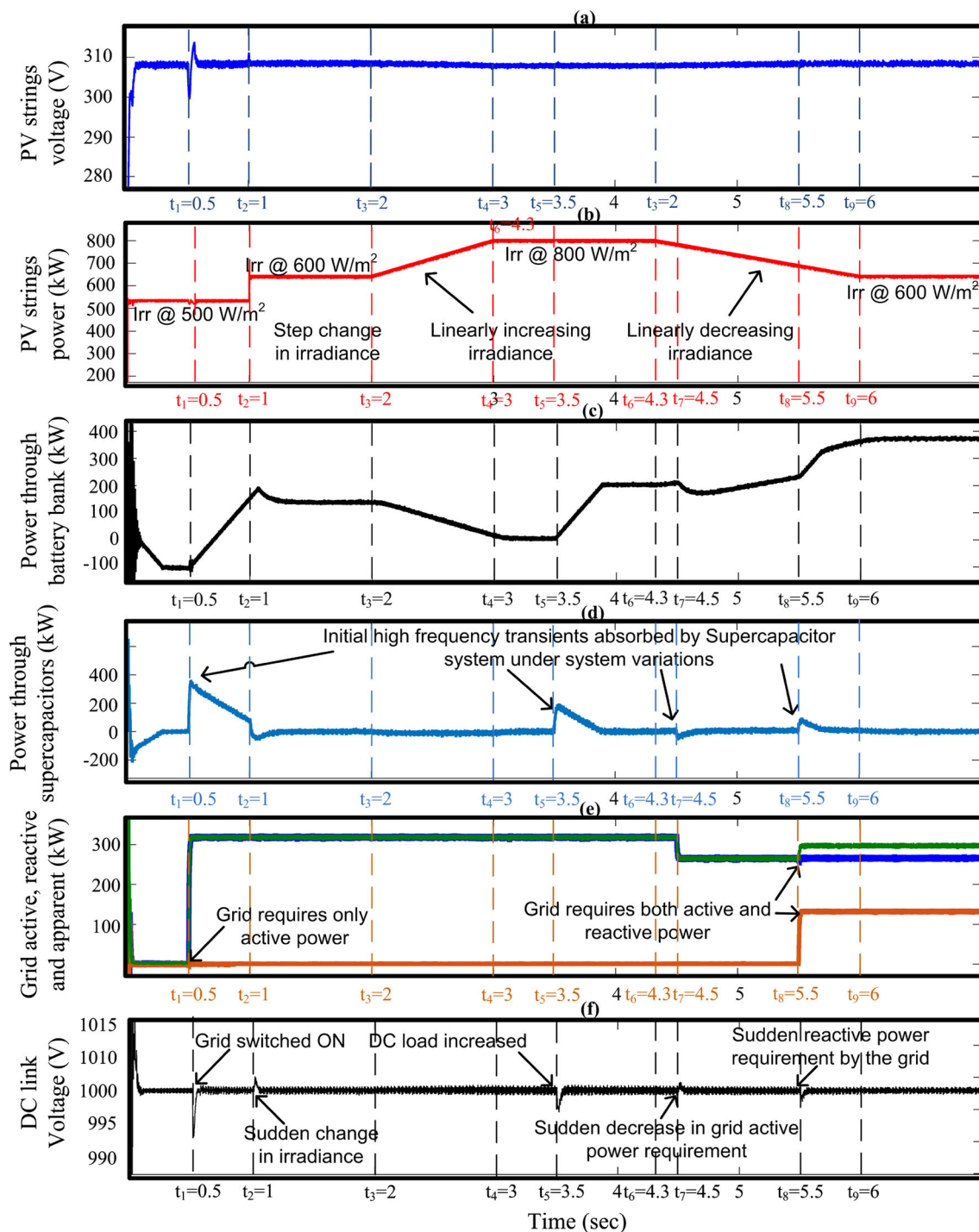


Fig. 14 a Voltage generated by the PV strings using MPPT b Total power through the solar PV system including PV strings ‘A’ and ‘B’; c Power through the battery bank; d Power through the supercapac-

itor modules; e Apparent (Green), Active (Blue) and Reactive power (Brown) required by the grid; f DC-link voltage profile

power until loading condition is changed. It can be observed from Fig. 14f that the duration of start-up transient is significantly less and the sudden spike generated on the DC link voltage profile is well within the allowable range of $\pm 5\%$. Proper current sharing is maintained between battery bank and supercapacitor modules.

At time $t_1=0.5$ sec, the three phase 480 V, 50 Hz local power grid is connected to the microgrid system through a NPC DC–AC converter demanding 300 kW power at unity power factor. Figure 14 shows the instantaneous variations in power from the PV strings, power through the battery bank, power through supercapacitor, active and reactive power by the grid. During the time interval between $t_1=0.5$ and $t_2=1$ sec, battery discharges itself to maintain the power balance at the DC link while supercapacitor absorbs the sudden transients until battery reaches the steady state condition. It can be observed that the energy management controller effectively helps in suppressing the transients on the DC link capacitor through the proposed power sharing scheme. Instantaneous waveforms of three phase voltage and current at PCC is shown in Fig. 15. It can be observed that current waveform using dq frame controller shows more distortion than the $\alpha\beta$ frame controller.

At time $t_2=1$ sec, PV strings are subjected to sudden increase in solar irradiance from 500 W/m^2 to 600 W/m^2 . The MPPT controller instantaneously adapts to the sudden variation in environmental conditions to generate the voltage reference for the closed loop control system such that maximum power is extracted from the two PV strings. Figure 14 shows the power profile of PV strings, energy storage elements, active and reactive power through NPC and voltage profile at the DC link. It can be observed that there is an increase in power through the PV strings. Thus, the energy management controller controls the action of the dual energy storage system. At $t_2=1$ sec, supercapacitor comes into play to absorb the high frequency transient experienced by the DC link due to sudden change in PV output. The discharged power through supercapacitor is eventually taken up by the batteries due to power sharing mechanism. Consequently, battery bank discharges itself to reach to a new steady state value. Power demand by the grid and the DC load remains unchanged.

Between the time interval $t_3=2$ sec and $t_4=3$ sec, the solar irradiance linearly rises to 800 W/m^2 . MPPT controller effectively manages the power flow through the PV strings as seen in Fig. 14. Co-ordinated control of supercapacitor and battery

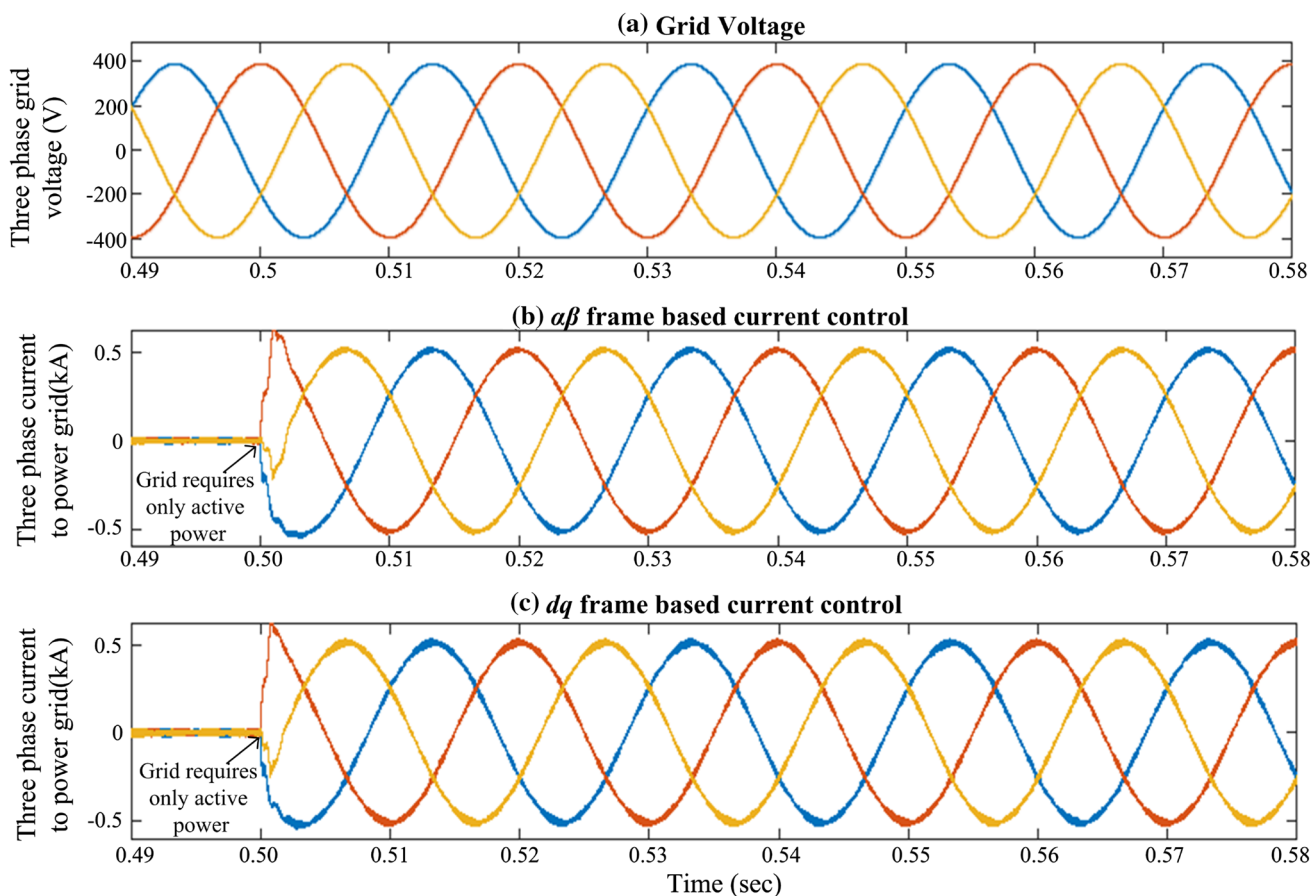


Fig. 15 Instantaneous 3- ϕ grid voltage and current waveform during start-up

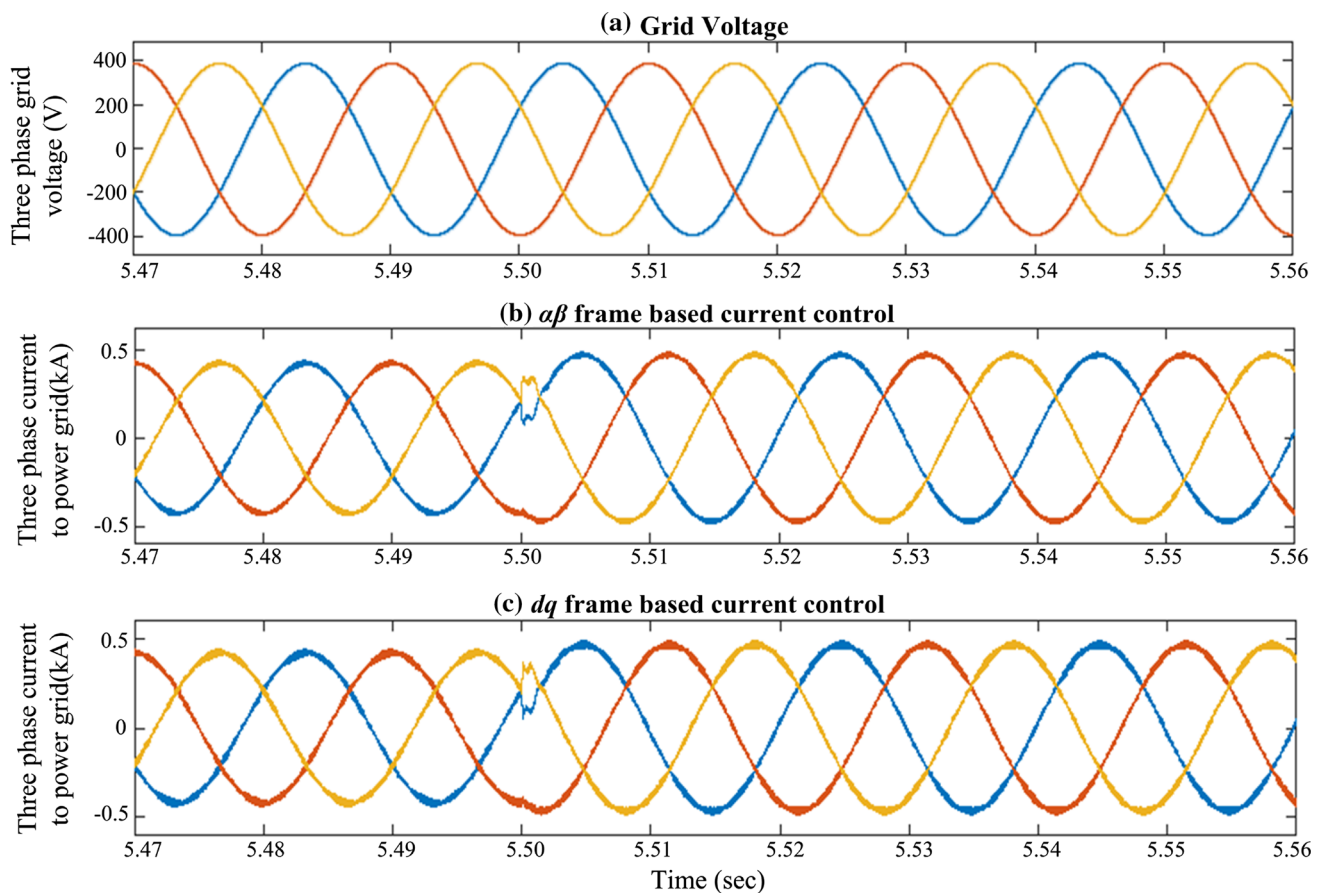


Fig. 16 Instantaneous 3- ϕ grid voltage and current waveform when both active and reactive power is demanded

suppresses the fluctuations experienced by the DC link capacitor. At time $t_5=3.5$ sec, a DC load of 200 kW is connected to the DC link while other parameters remains unchanged. High power transients are limited by the fast action of supercapacitor system. Energy management is effective in maintaining the power balance at the DC side. Between the time interval $t_6=4.3$ sec and $t_9=6$ sec, the irradiance level is decreasing linearly from 800 W/m^2 while the DC load demand remains unchanged. At time $t_7=4.5$ sec, the grid active power requirement is decreased to 50 kW. Grid side controller effectively controls the action of NPC converter to direct active power and reactive power to the main grid at PCC. Fig. 14 shows instantaneous variation of power through the microgrid components and voltage at the DC link. Instantaneous waveforms of three phase voltage and current at PCC is shown in Fig. 16. The distortion in the grid current waveform is significantly reduced using $\alpha\beta$ frame controller. The total harmonic distortion achieved using dq frame controller is obtained as 2.32% while for $\alpha\beta$ frame controller it is reduced to 1.65%. It can be observed from Fig. 17 that controller realized in $\alpha\beta$ frame compensates for the switching frequency harmonics better than the dq frame based current controller. Moreover, short duration transient is experienced by the DC link which

is eventually suppressed due to supercapacitor momentary action. As time increases, battery bank comes into play and discharges itself to manage the mismatch between generation and demand. At time $t_8=5.5$ sec, grid requires both active and reactive power. Co-ordinated control action effectively manages the power balance in the system as shown in Fig. 14. Supercapacitor takes care of the momentary fluctuations in the DC link voltage while the battery bank manages the steady state flow further.

Figure 18 shows individual battery voltage and state of charge. It can be observed that the terminal voltage of the battery always lies in the allowable range between 45 V and 55 V. This corresponds to favourable operating condition for battery's health/lifetime. Additionally, the proposed power sharing scheme helps in enhancing the battery lifespan as the battery charging/discharging current is limited under sudden power fluctuations which can be observed from individual battery's SOC profile shown in Fig. 18. A smooth time-series transition is observed in battery state of charge profile under charging and discharging cycles. The transients developing on the DC link capacitor are subsequently absorbed by the supercapacitor modules. Overall, the performance of the hybrid AC–DC microgrid with dual energy storage is com-

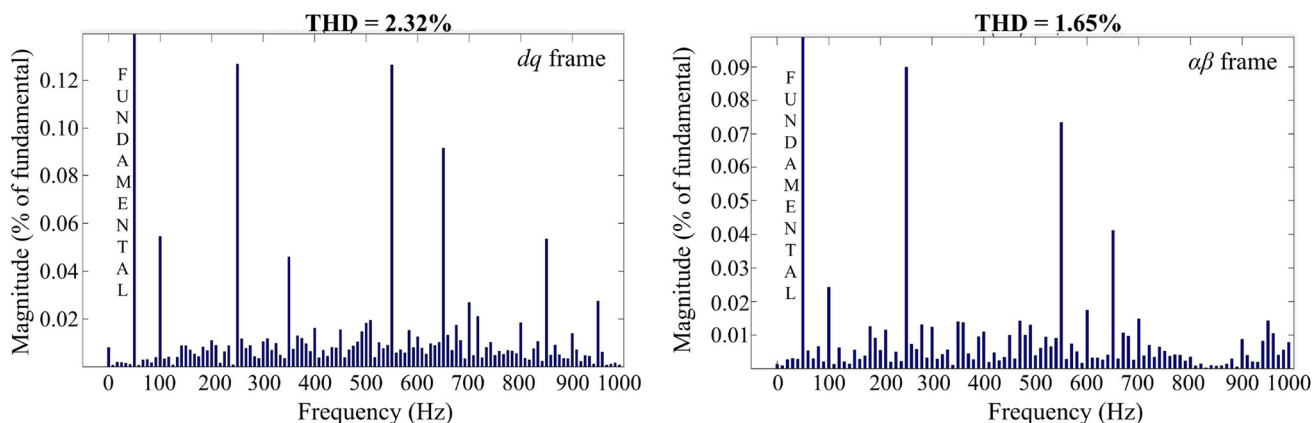
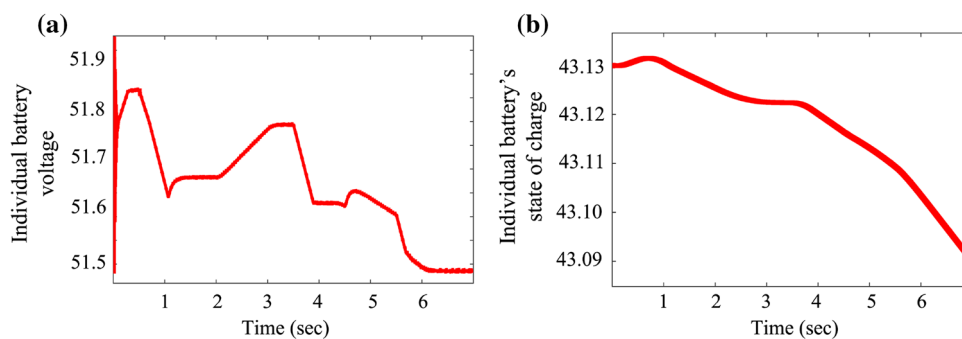


Fig. 17 Harmonic contents in grid current waveform using dq reference frame and $\alpha\beta$ reference frame controller

Fig. 18 **a** Instantaneous variation of individual battery voltage; **b** Instantaneous variation of individual battery state of charge



pared with the existing control technique. Table 4 shows the comparison based on DC link deviation and total harmonic distortion.

A real time validation of the proposed energy management control is performed on OPAL-RT platform as shown in Fig. 19. OP4510 simulator is used to demonstrate the performance of energy management controller in real time loading conditions. OP4510 has 96 digital and analog I/O channels. The processors allows a maximum allowable sampling time of $10\mu s$. Workstation enabled with RT-Lab interface MATLAB and OP4510 to generate the system response in real time. System response is obtained on digital signal oscilloscope through analog output channels. The effectiveness of the energy management controller is investigated in a converter based AC–DC microgrid consisting of solar PV, batteries and supercapacitors. At $t = T_1$ sec, solar irradiance is changed from 600 kW/m^2 to 1000 kW/m^2 . This sudden change is sensed by the controllers to activate the supercapacitors for the suppression of DC link voltage as shown in Fig. 20. At $t = T_2$ sec, there is a step increase in the grid active power requirement as shown in Fig. 21. The phase 'A' grid voltage and current is also shown. Supercapacitors momentarily supplies the load power before the battery discharges itself to reach a new steady state value. The DC link voltage is maintained constant at 1 kV. At $t = T_3$ sec, DC link experiences step increase in DC load as shown in Fig. 20.

Impact of increased DC load on DC link is mitigated by the co-ordinated management of batteries and supercapacitors.

9 Conclusions

The performance of the solar photovoltaic based hybrid AC–DC microgrid with dual energy storage system can be justified from the transient behaviour of the system under different loading and meteorological conditions considered in the results section. Additionally, real time validation of the multi agent AC–DC microgrid is also performed through OPAL RT and MATLAB interface. The role of efficient power conversion is vital in stable operation of the microgrid involving number of power sources. The closed loop control of power electronics converter improves the transient response of the microgrid. The PV side control including MPPT and a PID controller is observed to be efficient and robust under varying solar radiation profile. The Energy management controller is efficient and responsive in controlling the action of battery bank and supercapacitor modules using proposed power sharing scheme. Additionally, effective DC voltage regulation is achieved using synchronized action of energy management and proportional-integral based DC link voltage controller. It can be seen from the DC link voltage profile that the maximum ripple obtained in DC link volt-

Table 4 Comparison of DC link voltage deviation and total harmonic distortion

		Existing control scheme	Proposed scheme
DC link voltage	<i>During start – up</i>	0.91	1.02
	Other loading conditions	0.91	0.8 – 0.9
Total harmonic Distortion	Grid current	2.1-3	1.65

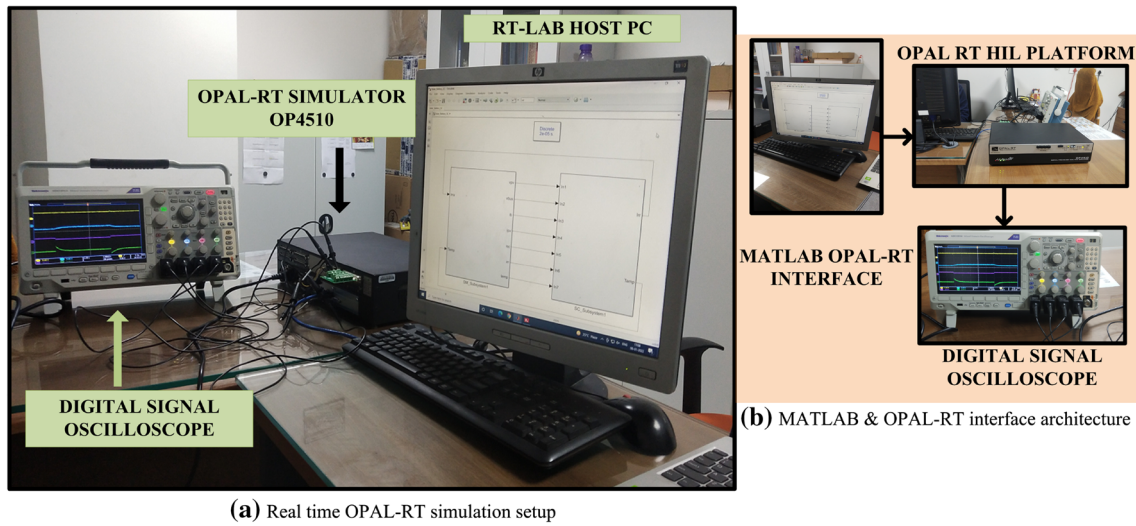


Fig. 19 Real time validation of energy management control in a AC–DC hybrid microgrid using MATLAB and OPAL-RT interface

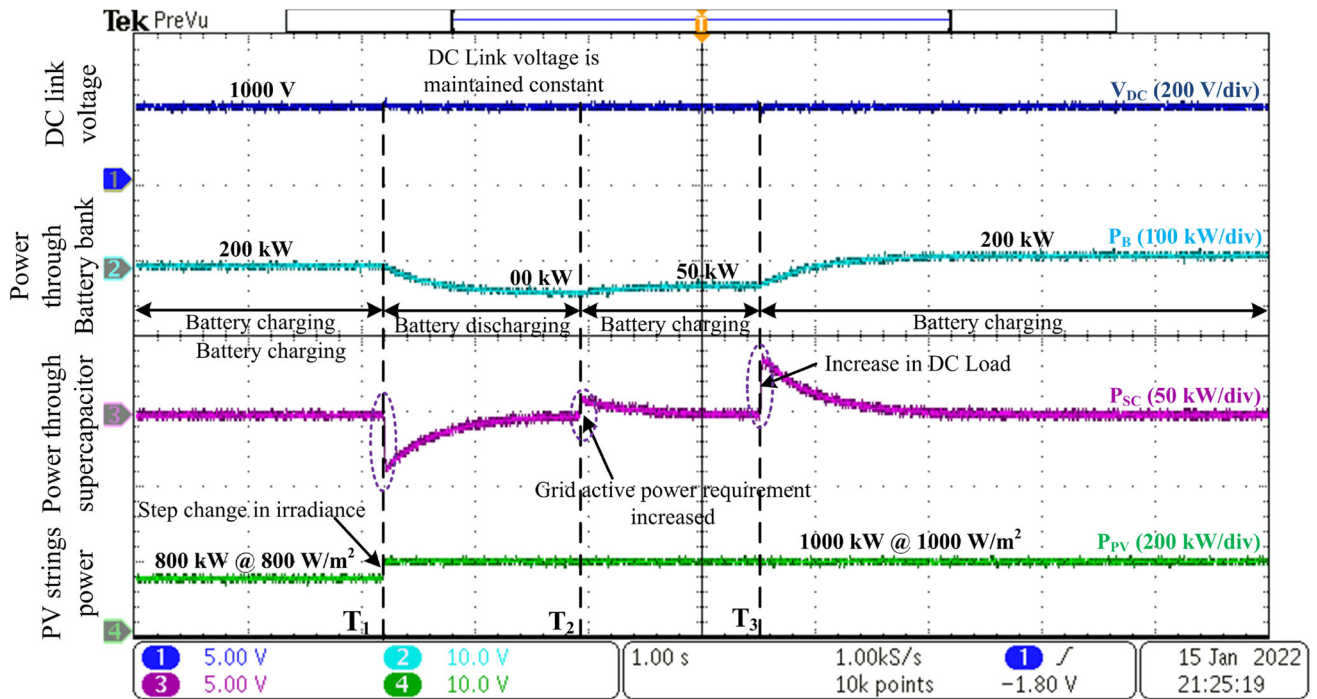


Fig. 20 Real time results showing DC link voltage profile, power through PV strings, batteries and supercapacitors

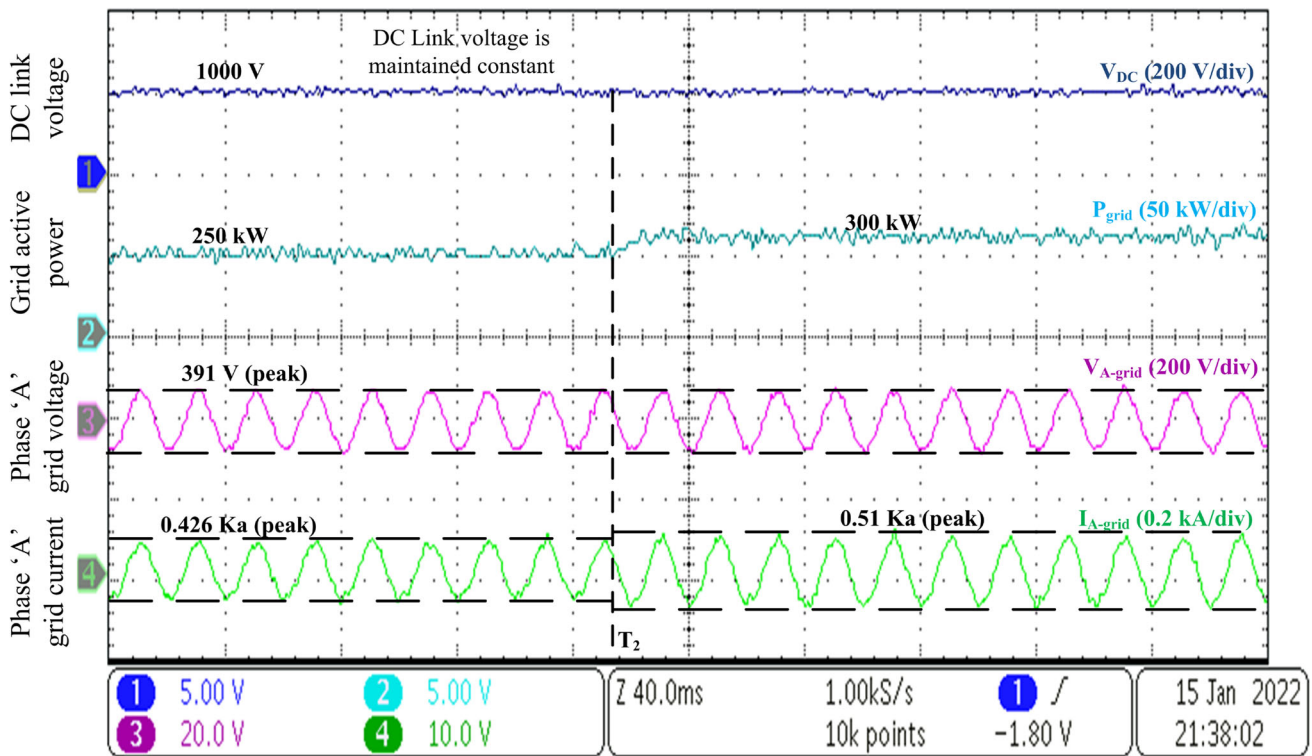


Fig. 21 Real time results showing DC link voltage profile, apparent power through the grid, phase ‘A’ grid voltage and current

age is well within the allowable limit of $\pm 5\%$. Grid side controller acts as a real and reactive power controller and controls the action of three phase neutral point clamped DC–AC converter to transmit both active and reactive power to the main grid. Higher order grid current controller ensures a better power quality and reduction in higher order harmonics. The performance of the hybrid AC–DC solar powered microgrid with dual energy storage is investigated under different real time loading conditions. The performance assessment of converter based microgrid with effective maximum power point tracking, efficient DC voltage regulation and reliable power sharing makes it suitable for solar and battery based distributed generation system. The results shows that proposed energy management:-

- Efficient regulation of DC link voltage.
- Enhancement in transient and dynamic response of the energy storage system
- Proper power sharing among hybrid power sources.
- Reduction in THD and improvement in grid power quality

Appendix A: Small Signal Model of Full Bridge Isolated PV Converter

A small signal model can be derived for solar PV panels connected to the DC through a Full bridge isolated DC–DC converter whose dynamics can mathematically expressed using equation (1) and (2). The control variable is the duty ratio expressed as d whereas two control variables are the inductor current through the converter and voltage across the input capacitor expressed as x_1, x_1 . equations (1) and (2) can be rewritten as

$$\frac{dx_1}{dt} = \frac{1}{L_{i1}} (d \cdot n \cdot x_2 - v_{DC-link}) = f_1(x_1, x_2, d) \quad (A1)$$

$$\frac{dx_2}{dt} = \frac{1}{C_{i1}} (i_{PV_i} - n \cdot d \cdot x_1) = f_2(x_1, x_2, d) \quad (A2)$$

Linearizing equations (A.1) and (A.2) at steady state condition, a small signal model can be expressed using equations (A.3) and (A.4)

$$\frac{d\tilde{f}_1}{dt} = \begin{pmatrix} \frac{\partial f_1}{\partial x_1} & \frac{\partial f_1}{\partial x_2} & \frac{\partial f_1}{\partial d} \\ \frac{\partial f_2}{\partial x_1} & \frac{\partial f_2}{\partial x_2} & \frac{\partial f_2}{\partial d} \end{pmatrix}_{ats.s.} \tilde{x}_1 + \begin{pmatrix} \frac{\partial f_1}{\partial x_1} & \frac{\partial f_1}{\partial x_2} \\ \frac{\partial f_2}{\partial x_1} & \frac{\partial f_2}{\partial x_2} \end{pmatrix}_{ats.s.} \tilde{x}_2 + \begin{pmatrix} \frac{\partial f_1}{\partial d} \\ \frac{\partial f_2}{\partial d} \end{pmatrix}_{ats.s.} \tilde{d} \quad (A3)$$

$$\frac{d\tilde{f}_2}{dt} = \begin{pmatrix} \frac{\partial f_2}{\partial x_1} & x_2, d \\ & \text{at s.s.} \end{pmatrix} \tilde{x}_1 + \begin{pmatrix} \frac{\partial f_2}{\partial x_2} & x_1, d \\ & \text{at s.s.} \end{pmatrix} \tilde{x}_2 + \begin{pmatrix} \frac{\partial f_2}{\partial d} & x_1, x_2 \\ & \text{at s.s.} \end{pmatrix} \tilde{d} \tag{A4}$$

Computing and equating the values of partial derivatives, we get

$$\frac{d\tilde{f}_1}{dt} = 0 \cdot \tilde{x}_1 + \frac{n \cdot D}{L_{i1}} \tilde{x}_2 + \frac{n \cdot X_2}{L_{i1}} \tilde{d} \tag{A5}$$

$$\frac{d\tilde{f}_2}{dt} = -\frac{n \cdot D}{C_{i1}} \tilde{x}_1 + \frac{1}{C_{i1}} \left(\frac{\partial i_{PV_i}}{\partial x_1} \right) \tilde{x}_2 - \frac{n \cdot X_1}{C_{i1}} \tilde{d} \tag{A6}$$

The term $\partial i_{PV_i} / \partial x_1 = \partial i_{PV_i} / \partial v_{PV_i}$ can be termed as the dynamic conductance g_{PV_i} since current equation of a solar cell is implicit equation which is dependent on both i_{PV} and v_{PV} . Hence,

$$\left(\frac{\partial i_{PV_i}}{\partial x_1} \right) = \left(\frac{\partial i_{PV_i}}{\partial v_{PV_i}} \right) = \frac{1}{r_{PV_i}} \tag{A7}$$

where,

$$\left(\frac{\partial i_{PV_i}}{\partial x_1} \right) = \left(\frac{\partial i_{PV_i}}{\partial v_{PV_i}} \right) = \frac{1}{r_{PV_i}}, \tag{A8}$$

$$i_{PV_i} = N_{par} [i_{Ph_i} - i_o (e^{\frac{qv_{PV_i}}{N_{ser} \cdot k \cdot A \cdot T_c}} - 1)], \tag{A9}$$

$$r_{PV_i} = -\frac{N_{ser} \cdot k \cdot A \cdot T_c}{N_{par} \cdot q \cdot i_o} e^{-\left(\frac{qv_{PV_i}}{N_{ser} \cdot k \cdot A \cdot T_c}\right)} \tag{A10}$$

Considering $x_1 = i_{iL1}$, $x_2 = v_{PV_i}$ and $d = d_i$, equations (A5) and (A6) can be written as

$$\frac{d\tilde{i}_{iL1}}{dt} = 0 \cdot \tilde{i}_{iL1} + \frac{n \cdot D_i}{L_{i1}} \tilde{v}_{PV_i} + \frac{n \cdot V_{PV_i}}{L_{i1}} \tilde{d}_i \tag{A11}$$

$$\frac{d\tilde{v}_{PV_i}}{dt} = -\frac{n \cdot D_i}{C_{i1}} \tilde{i}_{iL1} + \frac{1}{r_{PV_i} \cdot C_{i1}} \tilde{v}_{PV_i} - \frac{n \cdot I_{iL1}}{C_{i1}} \tilde{d} \tag{A12}$$

Obtaining laplace transform of equation (A11) and (A12), we get

$$s \cdot \tilde{i}_{iL1}(s) = \frac{n \cdot D_i}{L_{i1}} \tilde{v}_{PV_i}(s) + \frac{n \cdot V_{PV_i}}{L_{i1}} \tilde{d}(s) \tag{A13}$$

$$s \cdot \tilde{v}_{PV_i}(s) = -\frac{n \cdot D_i}{C_{i1}} \tilde{i}_{iL1}(s) + \frac{1}{r_{PV_i} \cdot C_{i1}} \tilde{v}_{PV_i}(s) - \frac{n \cdot I_{iL1}}{C_{i1}} \tilde{d}(s) \tag{A14}$$

References

1. Anthony, B., Jr.: Smart city data architecture for energy prosumption in municipalities: concepts, requirements, and future direc-

tions. *Int. J. Green Energy* **17**(13), 827–845 (2020). <https://doi.org/10.1080/15435075.2020.1791878>

2. International Renewable Energy Agency - IRENA . Future of solar photovoltaic. (2019)

3. Howarth, N.; Galeotti, M.; Lanza, A.; Dubey, K.: Economic development and energy consumption in the GCC: an international sectoral analysis. *Energy Trans.* (2017). <https://doi.org/10.1007/s41825-017-0006-3>

4. Delboni, L.F.; Marujo, D.; Balestrassi, P.P.; Oliveira, D.Q.: Electrical power systems: evolution from traditional configuration to distributed generation and microgrids. pp. 1–25. Springer International Publishing, Berlin (2018) (2018)

5. Petinrin, J.O.; Shaabanb, M.: Impact of renewable generation on voltage control in distribution systems (2016)

6. Gielen, D.; Boshell, F.; Saygin, D.; Bazilian, M.D.; Wagner, N.; Gorini, R.: The role of renewable energy in the global energy transformation. *Energ. Strat. Rev.* **24**, 38–50 (2019). <https://doi.org/10.1016/j.esr.2019.01.006>

7. Blanco, H.; Faaij, A.: A review at the role of storage in energy systems with a focus on Power to Gas and long-term storage (2018)

8. Rangarajan, S.S.; Collins, E.R.; Fox, J.C.; Kothari, D.P.: A survey on global PV interconnection standards. In: Institute of Electrical and Electronics Engineers Inc. (2017)

9. Al-Shetwi, A.Q.; Sujod, M.Z.: Grid-connected photovoltaic power plants: a review of the recent integration requirements in modern grid codes. *Int. J. Energy Res.* **42**(5), 1849–1865 (2018). <https://doi.org/10.1002/er.3983>

10. Elsayed, A.T.; Mohamed, A.A.; Mohammed, O.A.: DC microgrids and distribution systems: An overview (2015)

11. Yazdani, A.; Iravani, R.: *Electronic Power Conversion*. pp. 1–20. John Wiley and Sons, Inc., Hoboken (2010)

12. Bajaj, M.; Singh, A.K.: Grid integrated renewable DG systems: a review of power quality challenges and state-of-the-art mitigation techniques. *Int. J. Energy Res.* **44**(1), 26–69 (2020). <https://doi.org/10.1002/er.4847>

13. Xiao, W.; Moursi, M.S.; Khan, O.; Infield, D.: Review of grid-tied converter topologies used in photovoltaic systems (2016)

14. Blaabjerg, F.; Yang, Y.; Yang, D.; Wang, X.: *Distributed Power-Generation Systems and Protection* (2017)

15. Li, J.; Gee, A.M.; Zhang, M.; Yuan, W.: Analysis of battery lifetime extension in a SMES-battery hybrid energy storage system using a novel battery lifetime model. *Energy* **86**, 175–185 (2015). <https://doi.org/10.1016/j.energy.2015.03.132>

16. Kollimalla, S.K.; Mishra, M.K.; Ukil, A.; Gooi, H.B.: DC grid voltage regulation using new HESS control strategy. *IEEE Trans. Sustain. Energy* **8**(2), 772–781 (2017). <https://doi.org/10.1109/TSTE.2016.2619759>

17. Lin, X.; Lei, Y.: Coordinated control strategies for SMES-battery hybrid energy storage systems. *IEEE Access* **5**, 23452–23465 (2017). <https://doi.org/10.1109/ACCESS.2017.2761889>

18. Jami, M.; Shafiee, Q.; Gholami, M.; Bevrani, H.: Control of a super- capacitor energy storage system to mimic inertia and transient response improvement of a direct current micro-grid Control of a super-capacitor energy storage system to mimic inertia and transient response improvement of a direct current micro-grid. *J. Energy Storage* **2020**(32), 101788 (2020). <https://doi.org/10.1016/J.EST.2020.101788>

19. Takagi, K.; Fujita, H.: Dynamic control and performance of an isolated dual-active-bridge DC–DC converter. In: Institute of Electrical and Electronics Engineers Inc.; pp. 1521-1527 (2015)

20. Kong, L.; Yu, J.; Cai, G.: Modeling, control and simulation of a photovoltaic /hydrogen/ supercapacitor hybrid power generation system for grid-connected applications. *Int. J. Hydrog. Energy* **44**(46), 25129–25144 (2019). <https://doi.org/10.1016/j.ijhydene.2019.05.097>

21. Senapati, M.K.; Pradhan, C.; Samantaray, S.R.; Nayak, P.K.: Improved power management control strategy for renewable energy based DC micro-grid with energy storage integration. *IET Gener. Transm. Distrib.* **13**(6), 838–849 (2019). <https://doi.org/10.1049/iet-gtd.2018.5019>
22. Xuan, Y.; Yang, X.; Chen, W.; Liu, T.; Hao, X.: A novel NPC dual-active-bridge converter with blocking capacitor for energy storage system. *IEEE Trans. Power Electron.* **34**(11), 10635–10649 (2019). <https://doi.org/10.1109/TPEL.2019.2898454>
23. Dubarry, M.; Pastor-Fernández, C.; Baure, G.; Yu, T.F.; Widanage, W.D.; Marco, J.: Battery energy storage system modeling: Investigation of intrinsic cell-to-cell variations. *J. Energy Storage* **23**, 19–28 (2019). <https://doi.org/10.1016/j.est.2019.02.016>
24. An, F.; Chen, L.; Huang, J.; Zhang, J.; Li, P.: Rate dependence of cell-to-cell variations of lithium-ion cells. *Sci. Rep.* **6**(1), 1–7 (2016). <https://doi.org/10.1038/srep35051>
25. Prasanna, U.R.; Rathore, A.K.: Small-signal modeling of active-clamped ZVS current-fed full-bridge isolated DC/DC converter and control system implementation using PSoC. *IEEE Trans. Industr. Electron.* **61**(3), 1253–1261 (2014). <https://doi.org/10.1109/TIE.2013.2259784>
26. Mahdavyfakhr, M.; Amiri, N.; Jatskevich, J.: Small Signal Modeling of Full Bridge Boost Converter. In: . 2019-June. Institute of Electrical and Electronics Engineers Inc.; pp. 985–989 (2019)
27. Yue, X.; Wang, X.; Blaabjerg, F.: Review of small-signal modeling methods including frequency-coupling dynamics of power converters. *IEEE Trans. Power Electron.* **34**(4), 3313–3328 (2019). <https://doi.org/10.1109/TPEL.2018.2848980>
28. MLU Series Photovoltaic Modules-Technical Specifications
29. Tan, X.; Li, Q.; Wang, H.: Advances and trends of energy storage technology in Microgrid. *Int. J. Electr. Power Energy Syst.* **44**(1), 179–191 (2013). <https://doi.org/10.1016/j.ijepes.2012.07.015>
30. Vargas, U.; Lazaroiu, G.C.; Tironi, E.; Ramirez, A.: Harmonic modeling and simulation of a stand-alone photovoltaic-batterysupercapacitor hybrid system. *Int. J. Electr. Power Energy Syst.* **105**, 70–78 (2019). <https://doi.org/10.1016/j.ijepes.2018.08.004>
31. Datasheet for RESU6.5-Technical specifications
32. Craciun, B.I.; Kerekes, T.; Séra, D.; Teodorescu, R.: Overview of recent grid codes for PV power integration. pp. 959–965 (2012)
33. Preda, T.N.; Uhlen, K.; Nordgård, D.: An overview of the present grid codes for integration of distributed generation. In: *Institution of Engineering and Technology (IET)*; p. 20 (2012)
34. Teodorescu, R.; Liserre, M.; Rodríguez, P.: *Grid Converters for Photovoltaic and Wind Power Systems*. John Wiley and Sons, Ltd., Chichester (2011)

